Collected images from the literature

Image	Comment

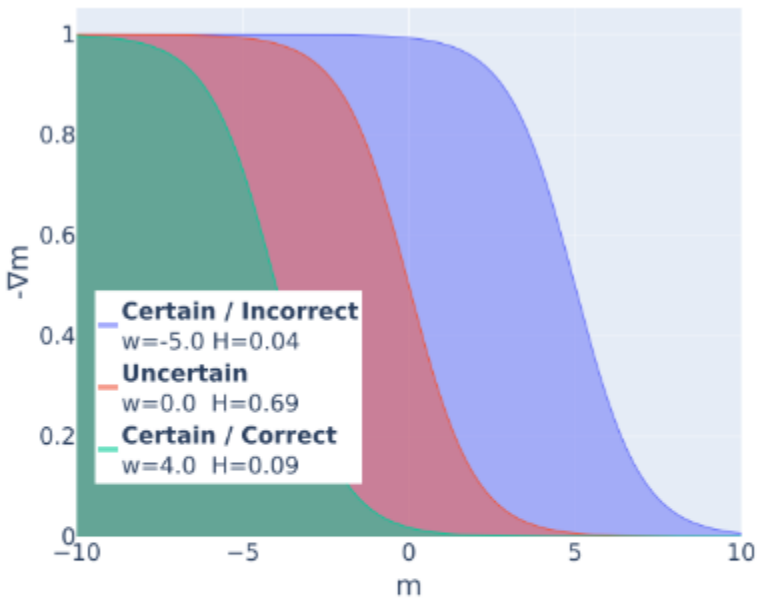

(a) Gradient update of m for different values of w on binary classification.

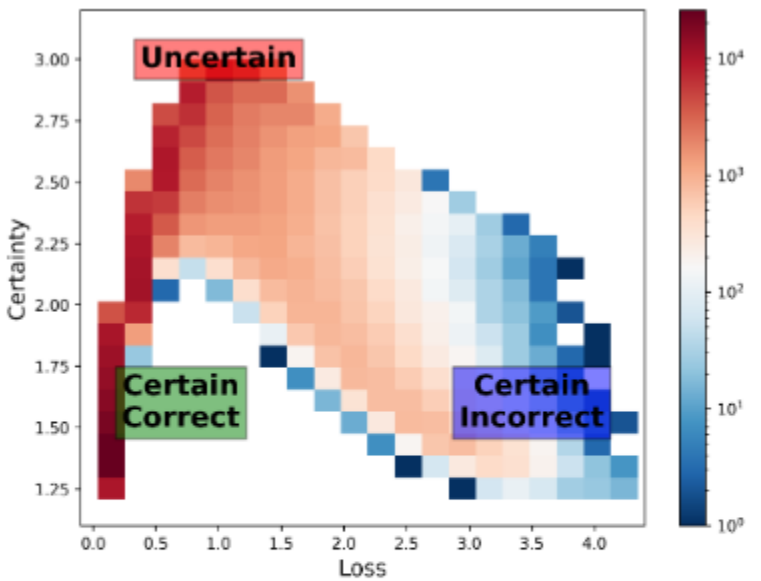

(b) 2D projection of MNLI examples from a trained weak learner. Colors indicate the concentration and are in log scale.

Figure 1: The analysis of the gradients reveals 3 regimes where the gradient is shifted by the certainty and correctness of the weak learner. These 3 regions are present in real dataset such as MNLI.

Image	Comment

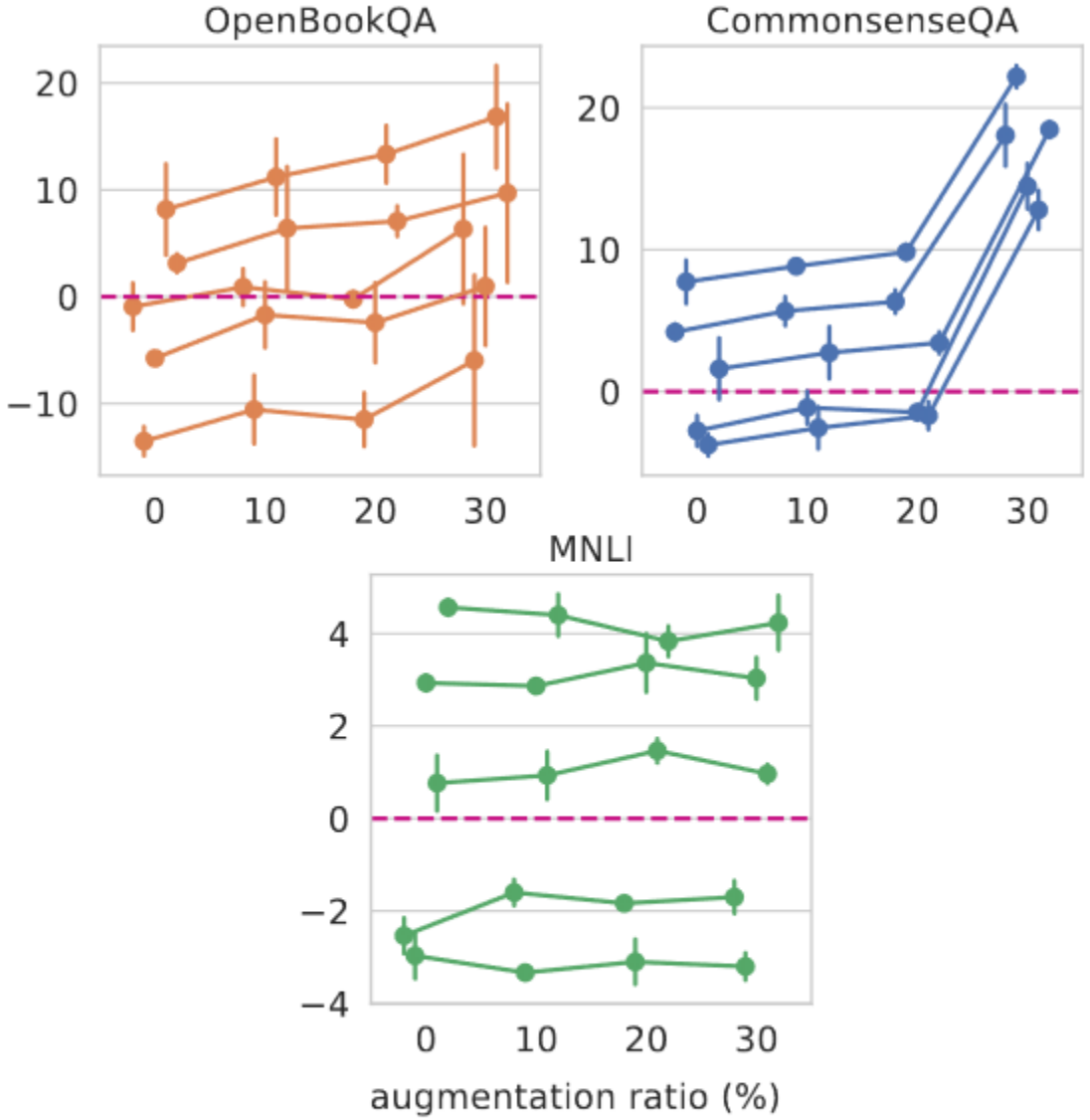

Figure 3: Performance difference between single-annotator splits and random splits of identical size. The x-axis indicates the fraction of examples taken from the development set to augment the training set.

Image	Comment

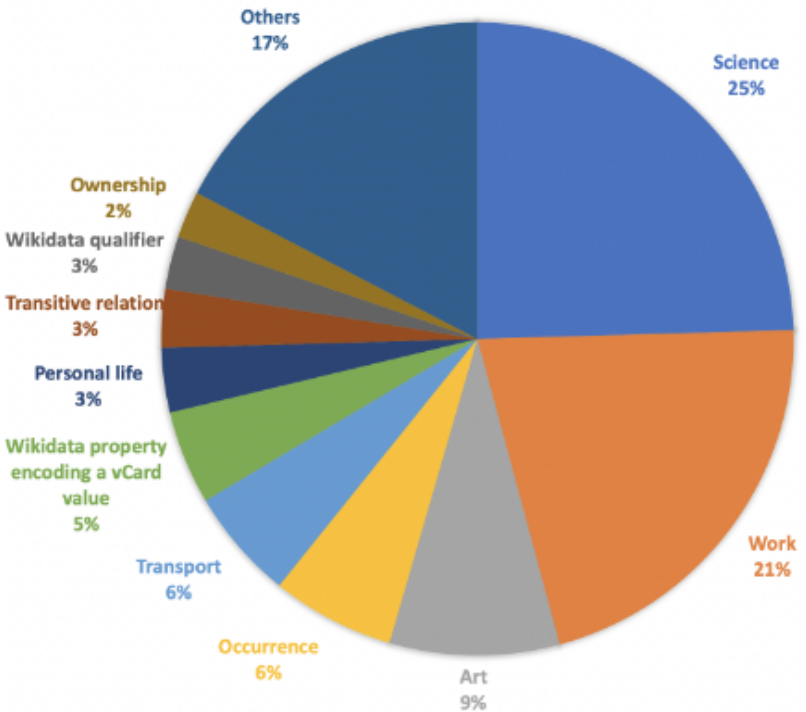

Figure 3: Relation domain distribution.

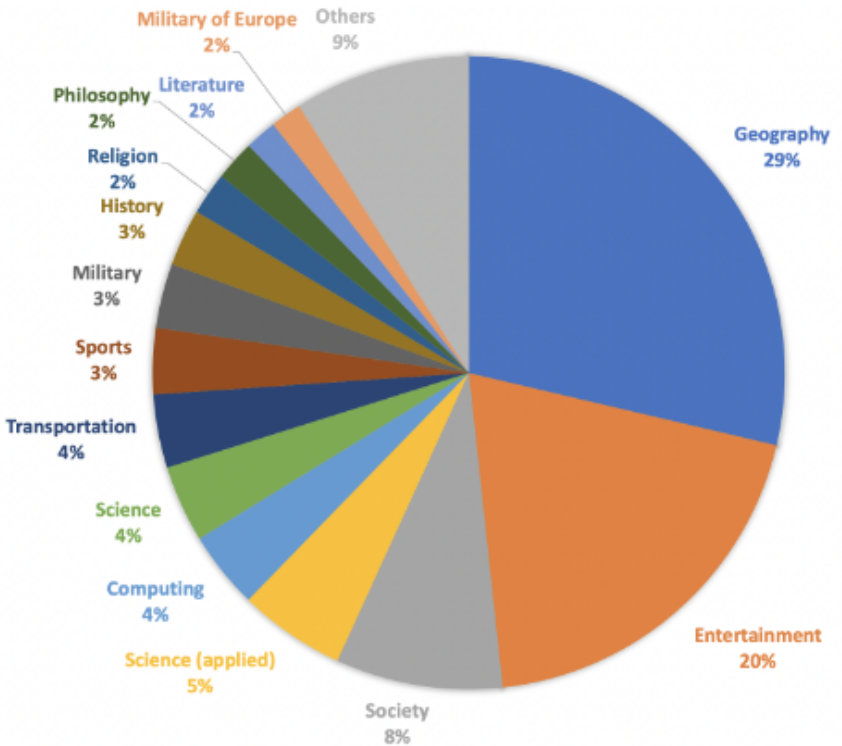

Figure 4: Document domain distribution.

Image	Comment

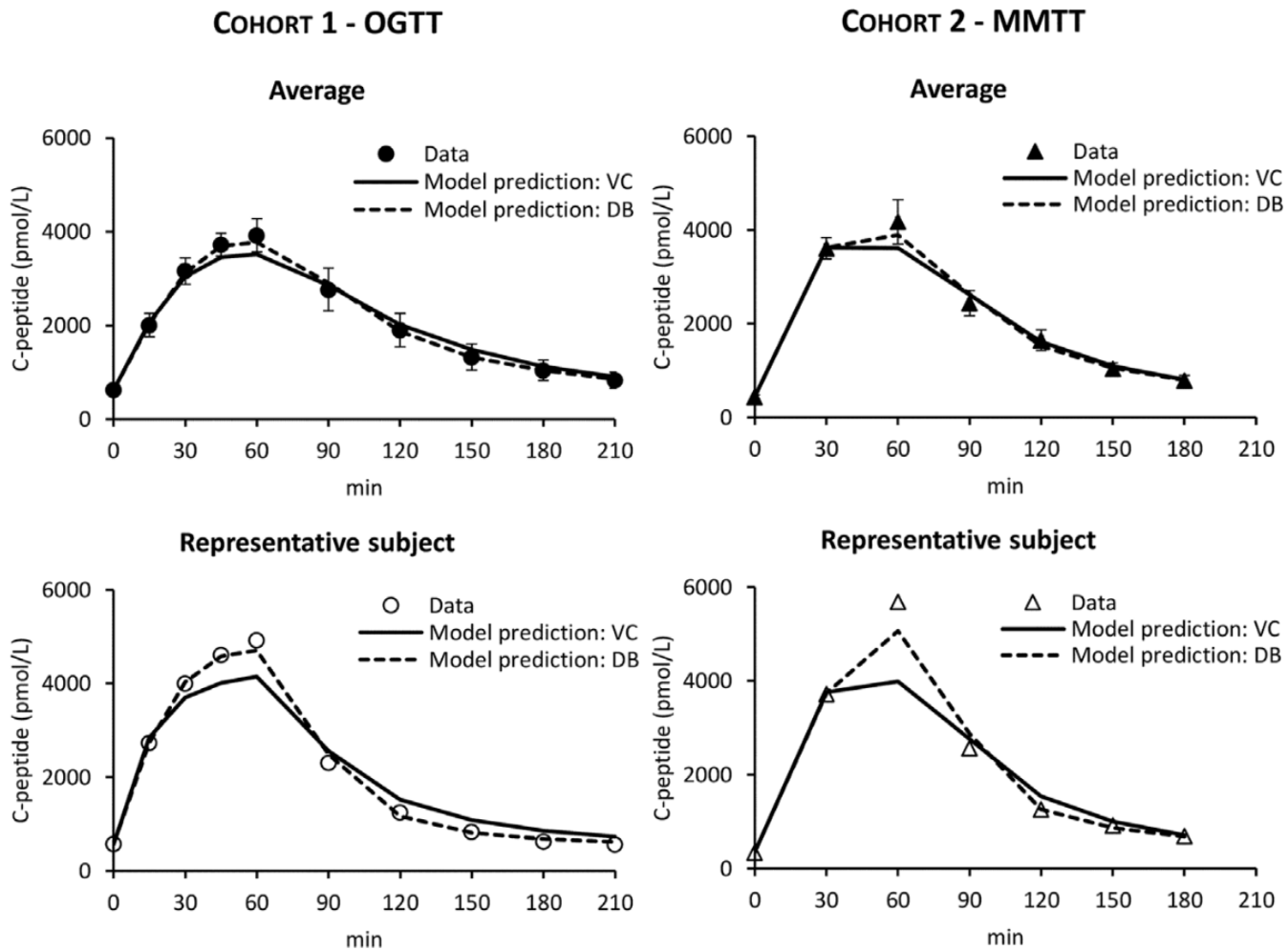

FIGURE 4 | C-peptide data in Cohort 1 – OGTT (left panels, circles) and Cohort 2 – MMTT (right panels, triangles) vs. model predictions obtained with VC (continuous line) and DB (dashed line) approach. Mean ± SE are reported in the top panels while representative subjects in the bottom panels.

Image	Comment

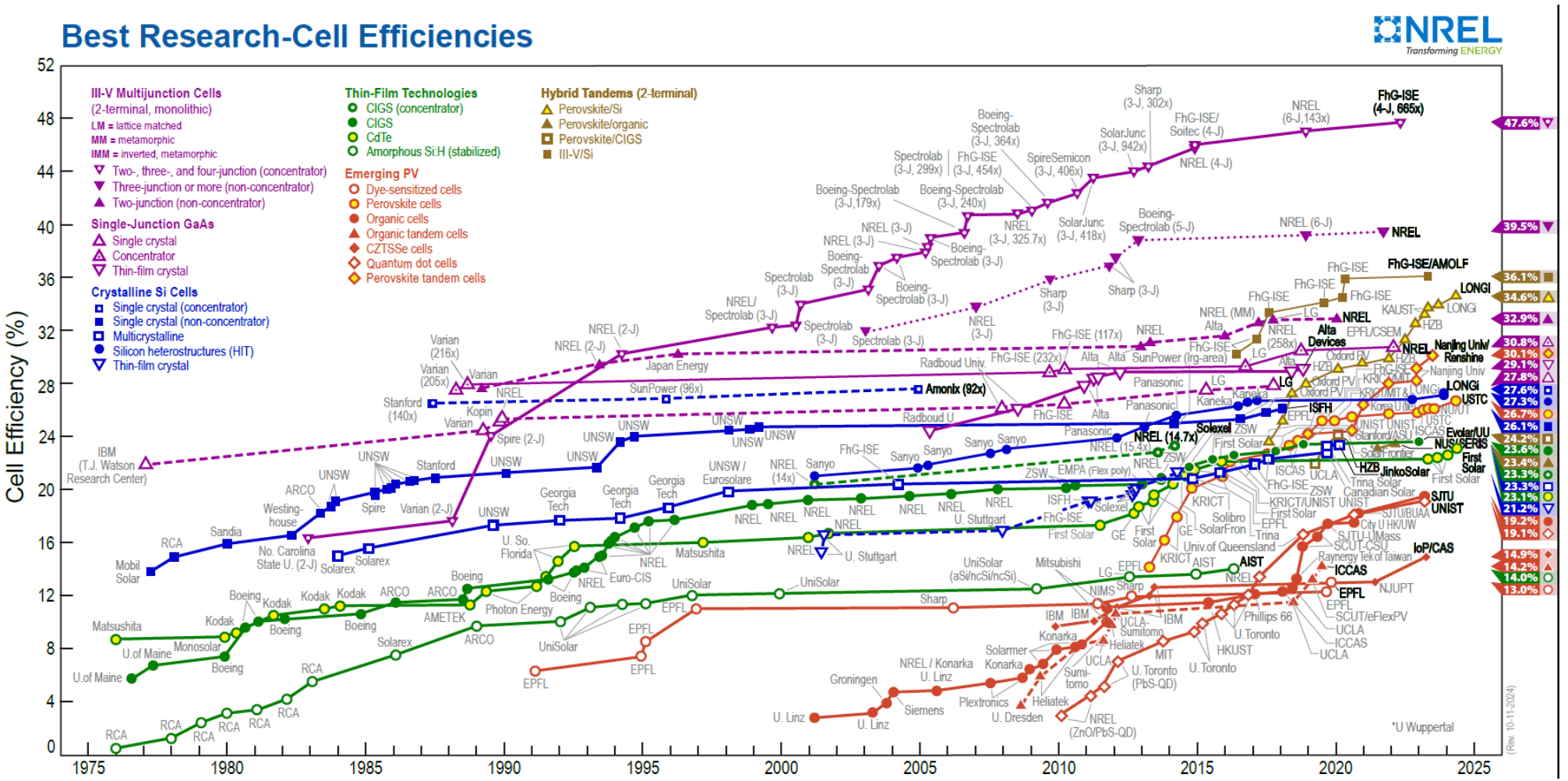

Image | Comment

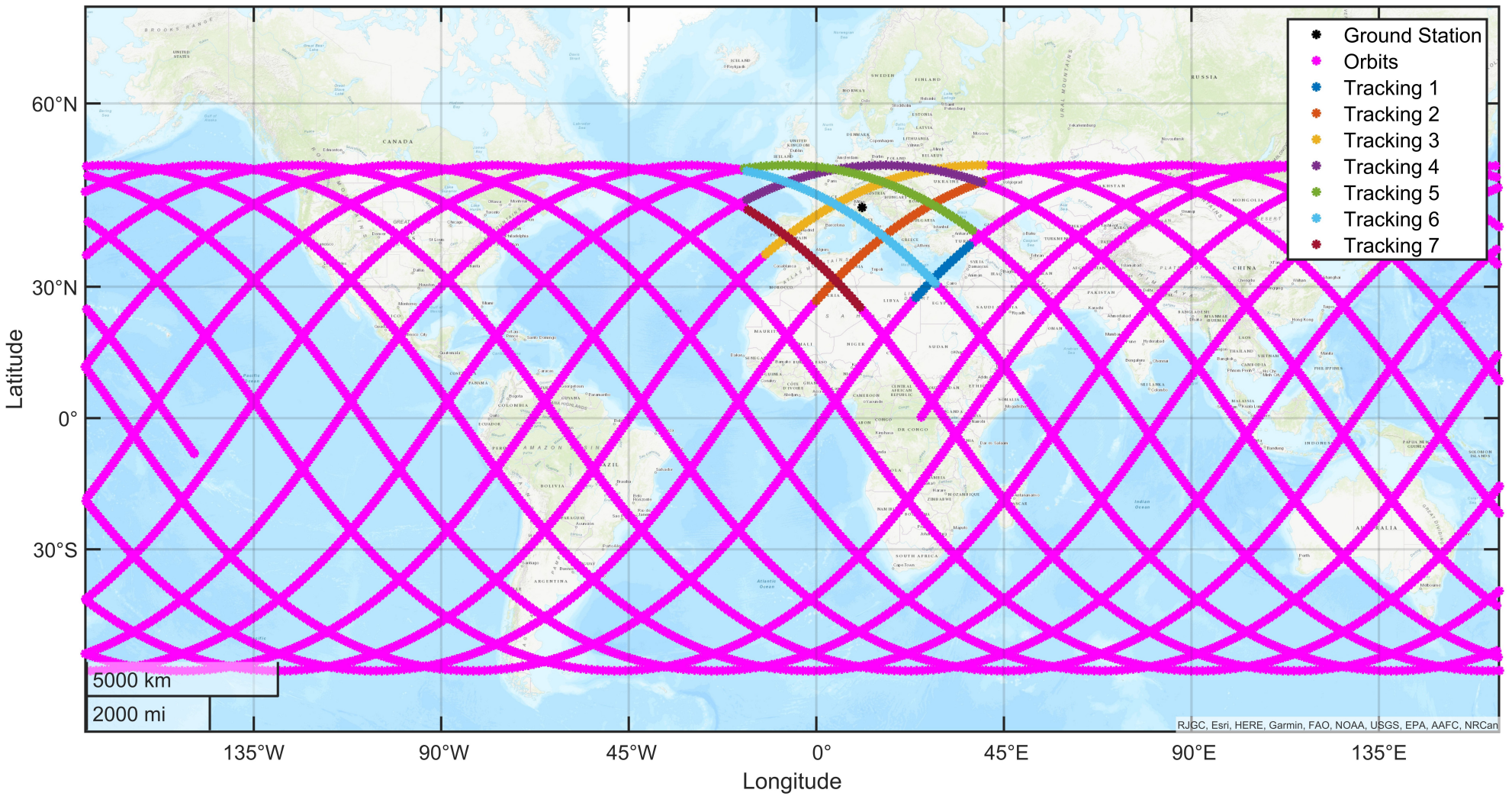

Image	Comment

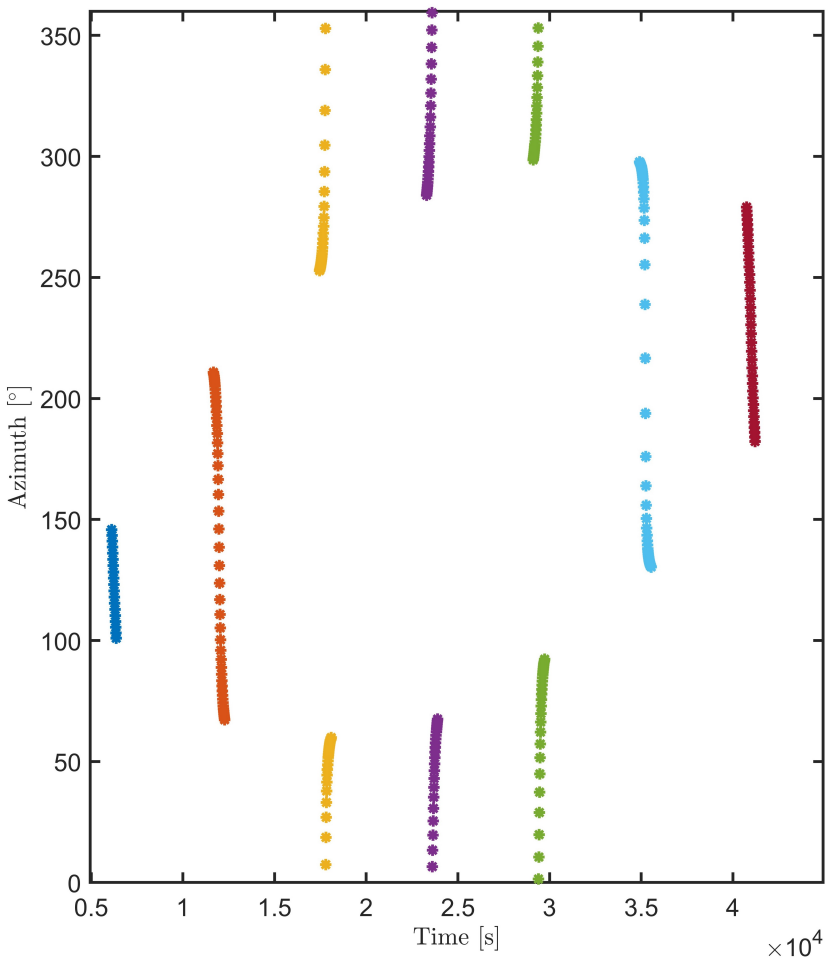

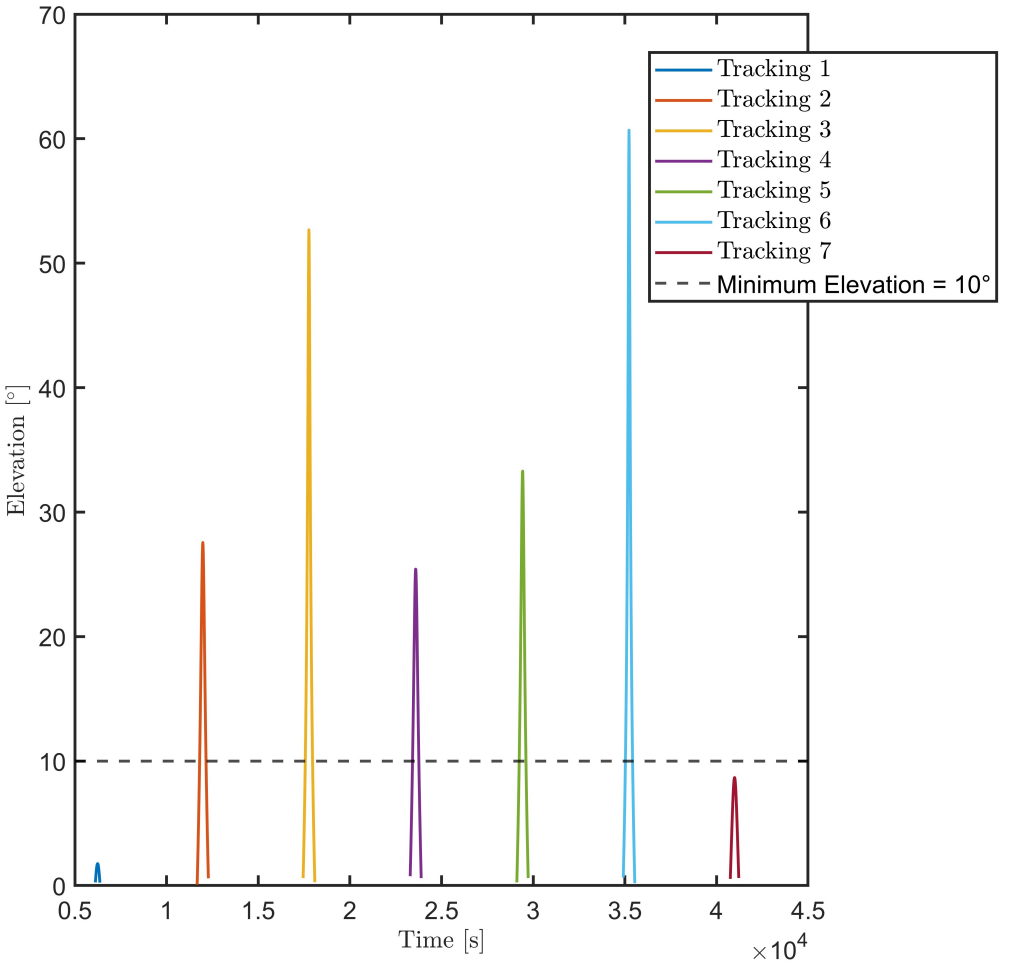

Image	Comment

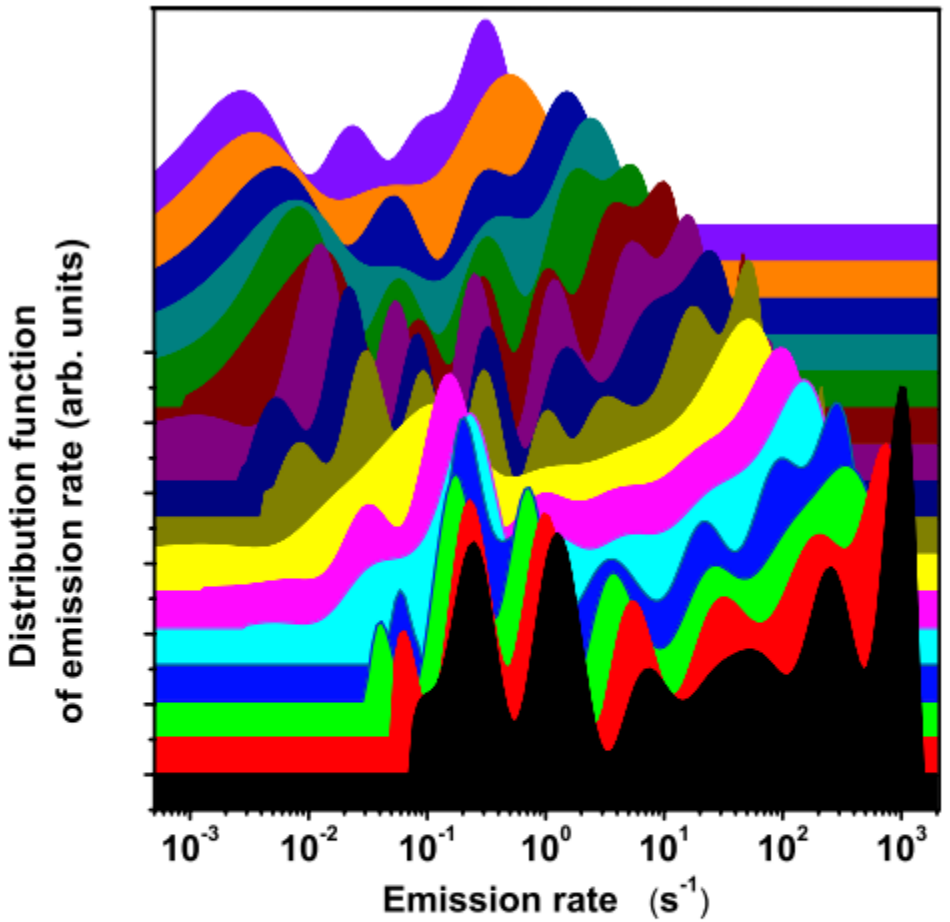

FIG. 6. (Color online) Distribution function $g(\ln W)$ of the emission rates for temperatures decreasing from 650 K at the bottom of the figure to 500 K at the top, with 10 K steps, deduced from applying the FTIKERG algorithm to the imaginary and the real isothermal spectra in Fig. 5 for boron-doped diamond (sample BM02).

Image	Comment

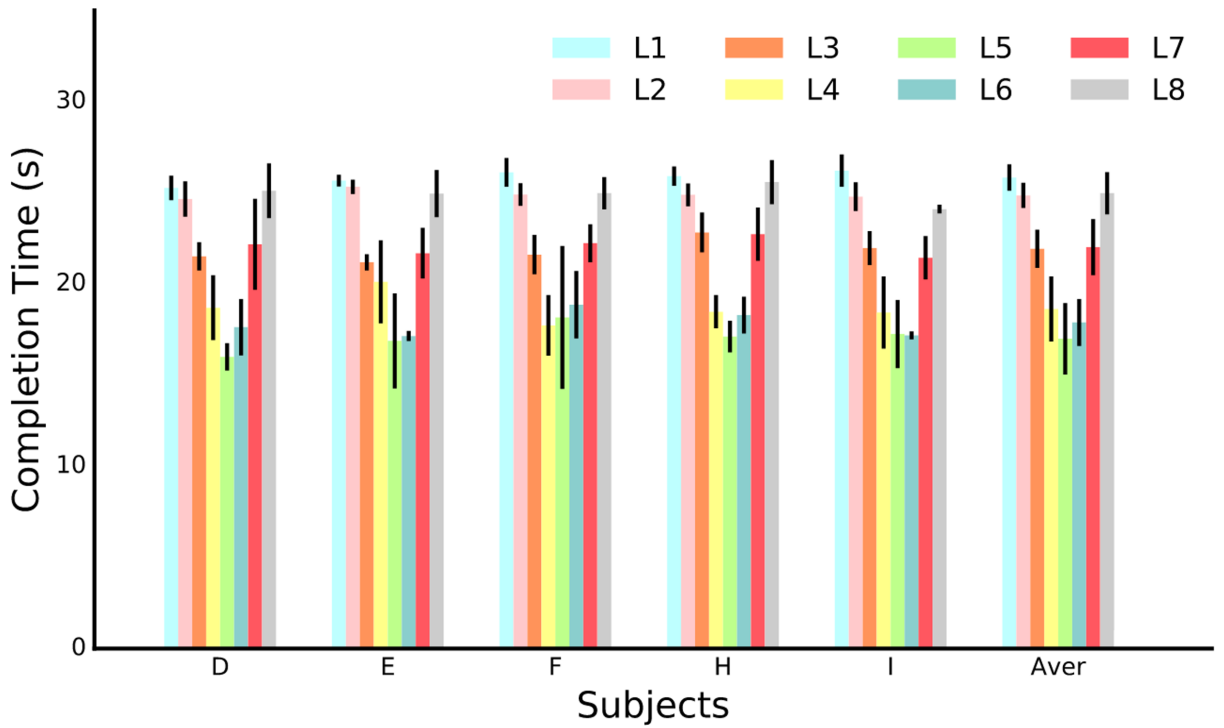

Fig. 6. Average completion time of each location in session 1. L1–L8 represents the eight locations which are shown in Fig. 3(a).

Pros:

- Colors used to differentiate the locations
- Keep always the same order of colors per subject
- Subjects represented with letters and not numbers (already used for locations)
- Black line is highlighted wrt to the bin
- Easy the comparison intra and inter subjects

Cons:

- Some of the color are not suitable to be transposed to grayscale, yellow and blue are probably too light

Image	Comment

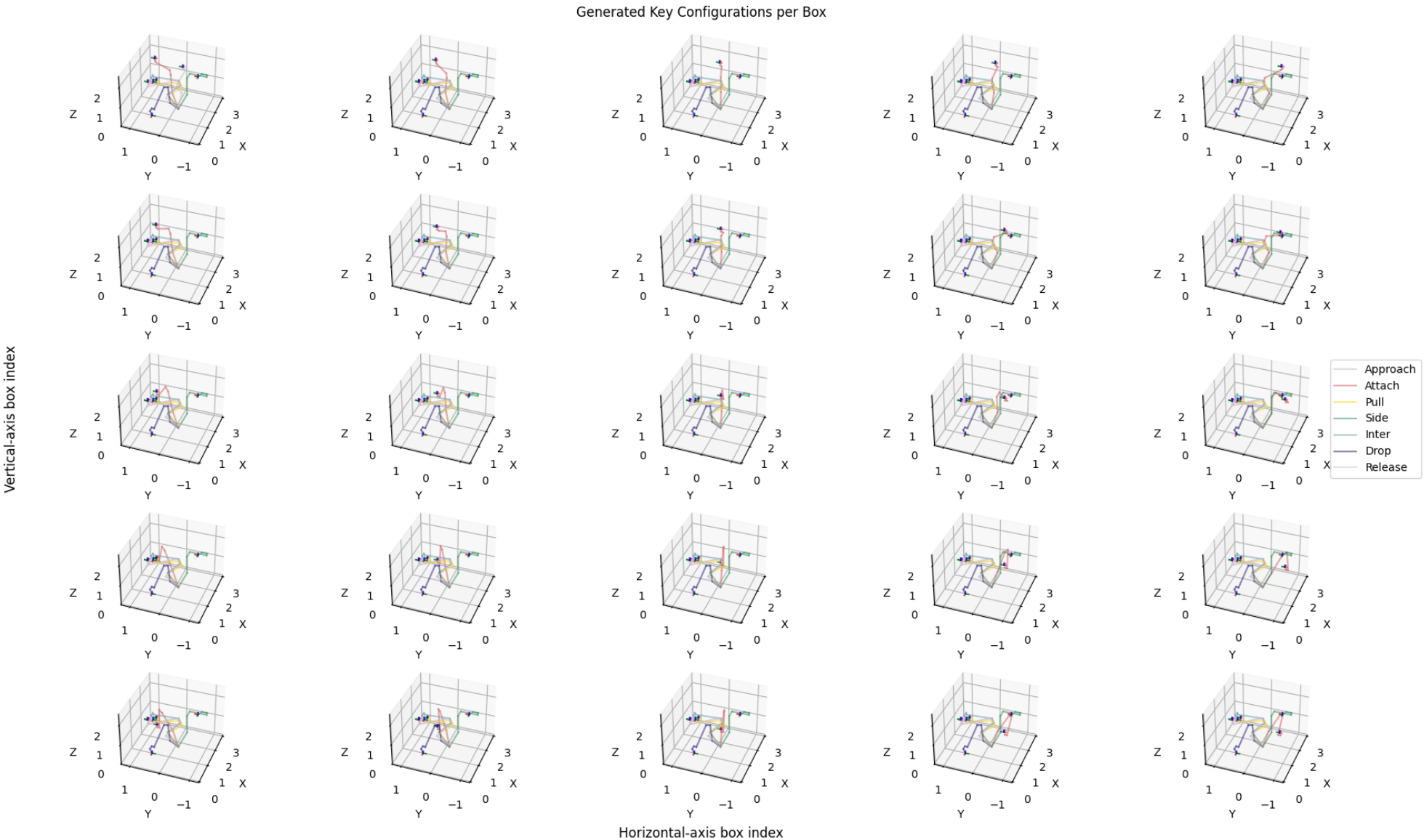

Image	Comment

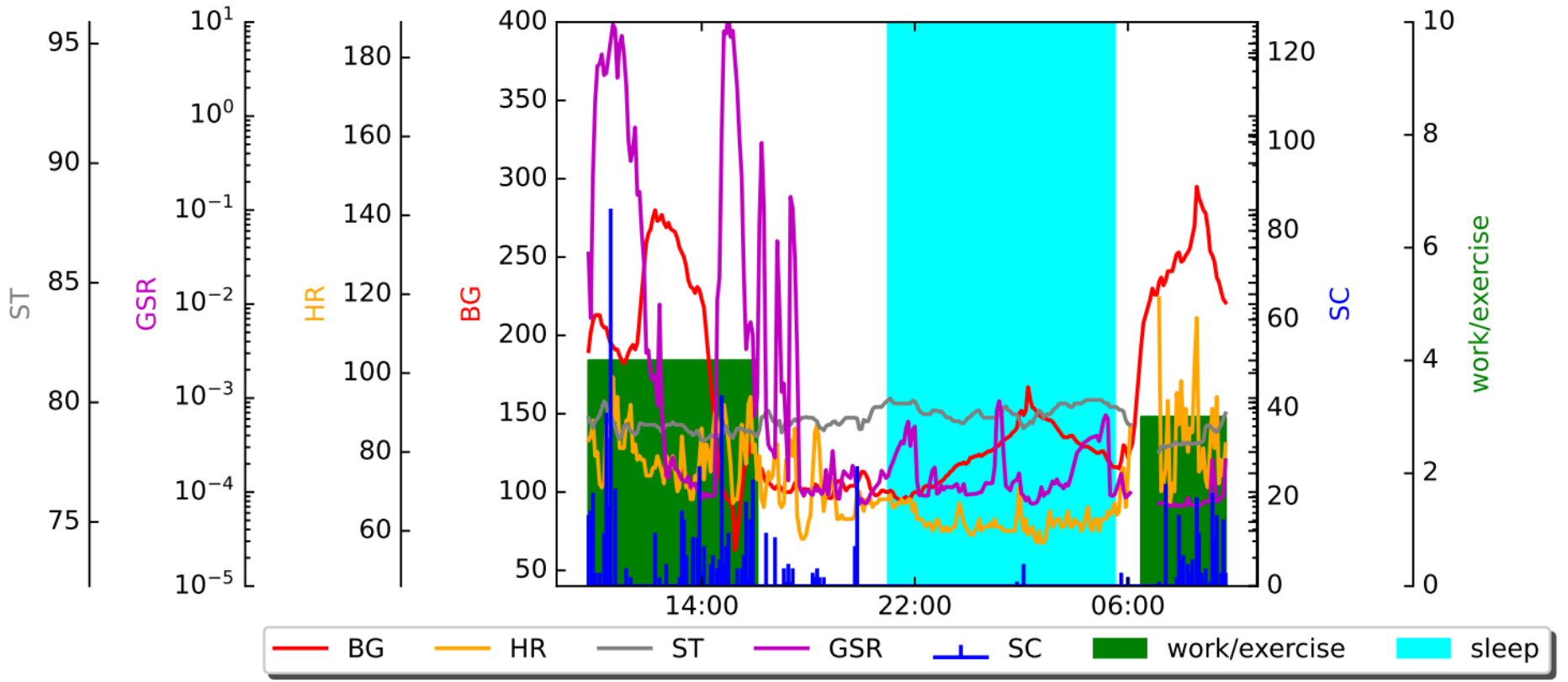

Fig. 1: A presentation of blood glucose level and physical activity-related data for PID 559 for a duration of 24 hours. Note. BG: blood glucose; HR: heart rate; GSR: galvanic skin response; ST: skin temperature; SC: step count.

Image | Comment

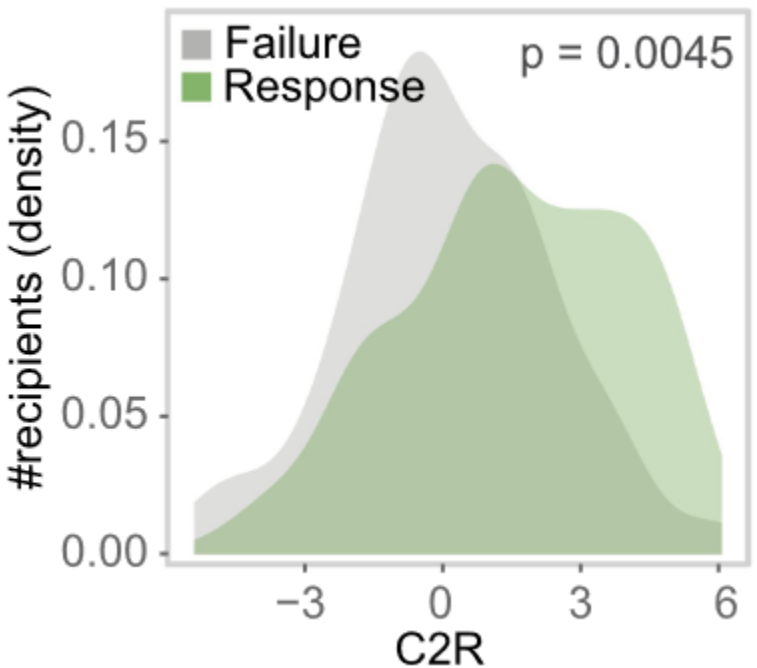

Image | Comment

g

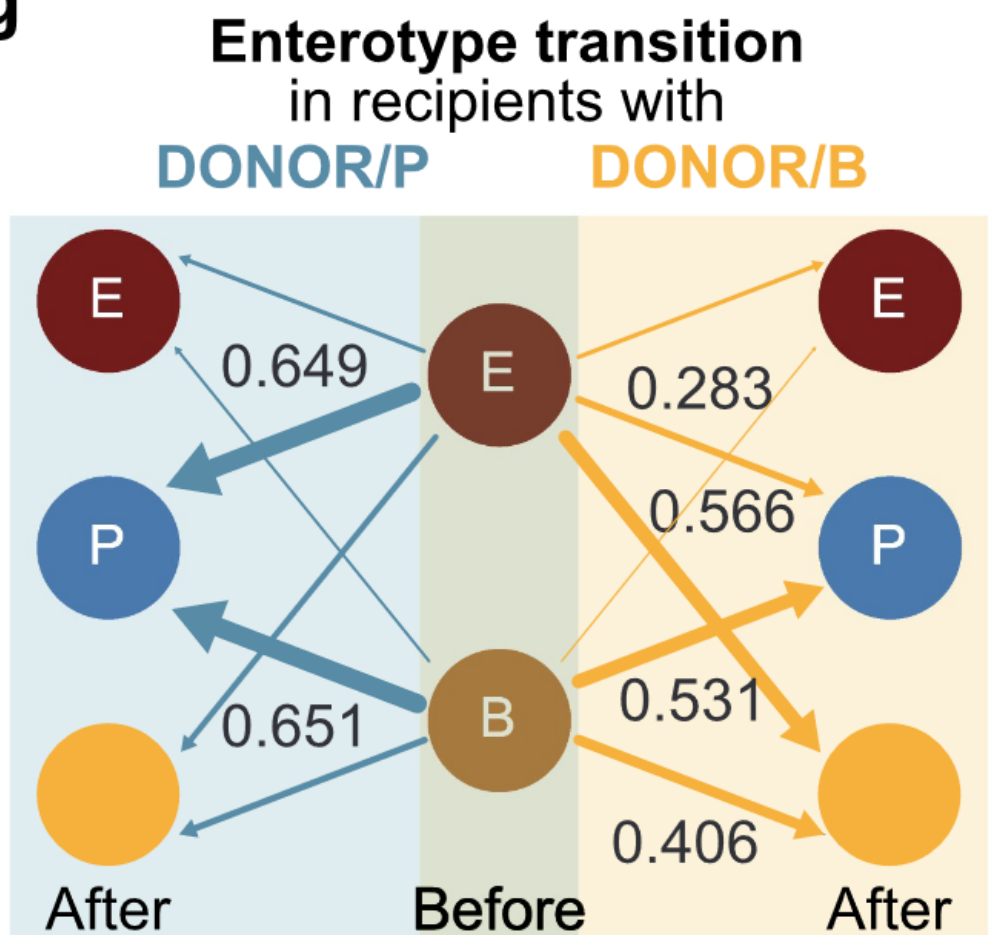

Image	Comment

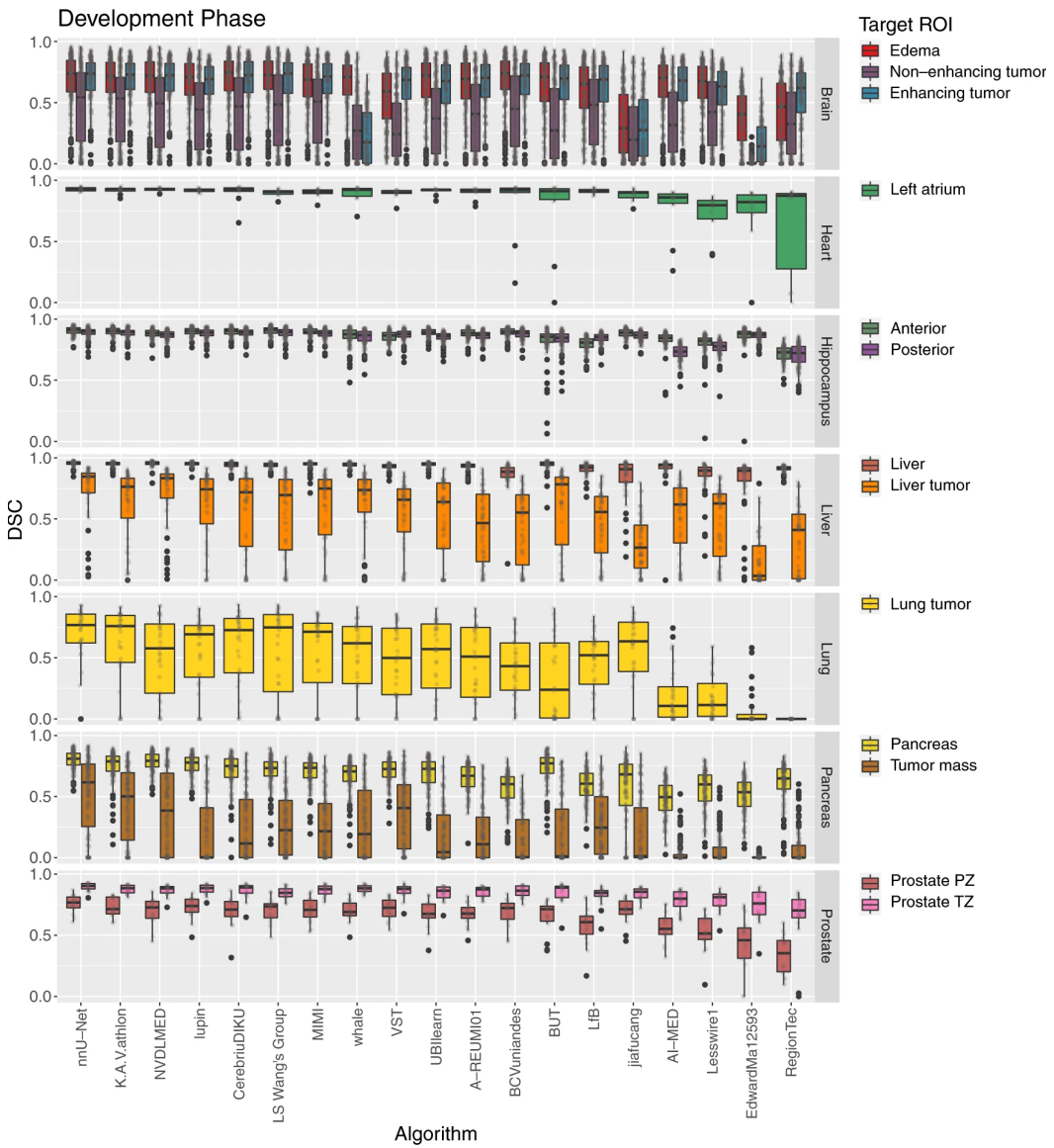

Image | Comment

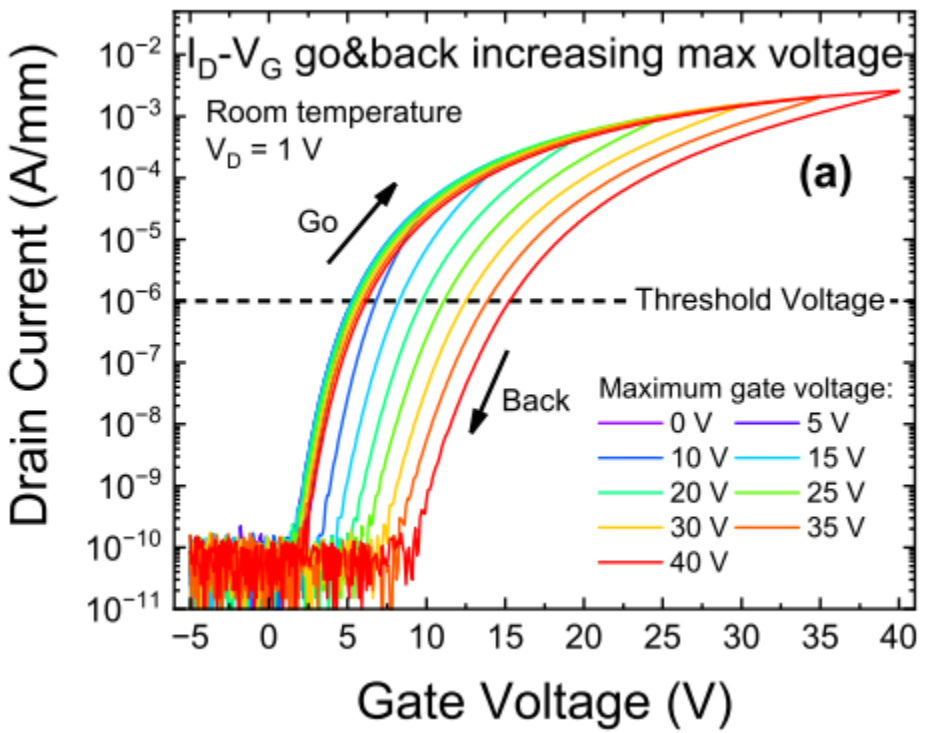

Image | Comment

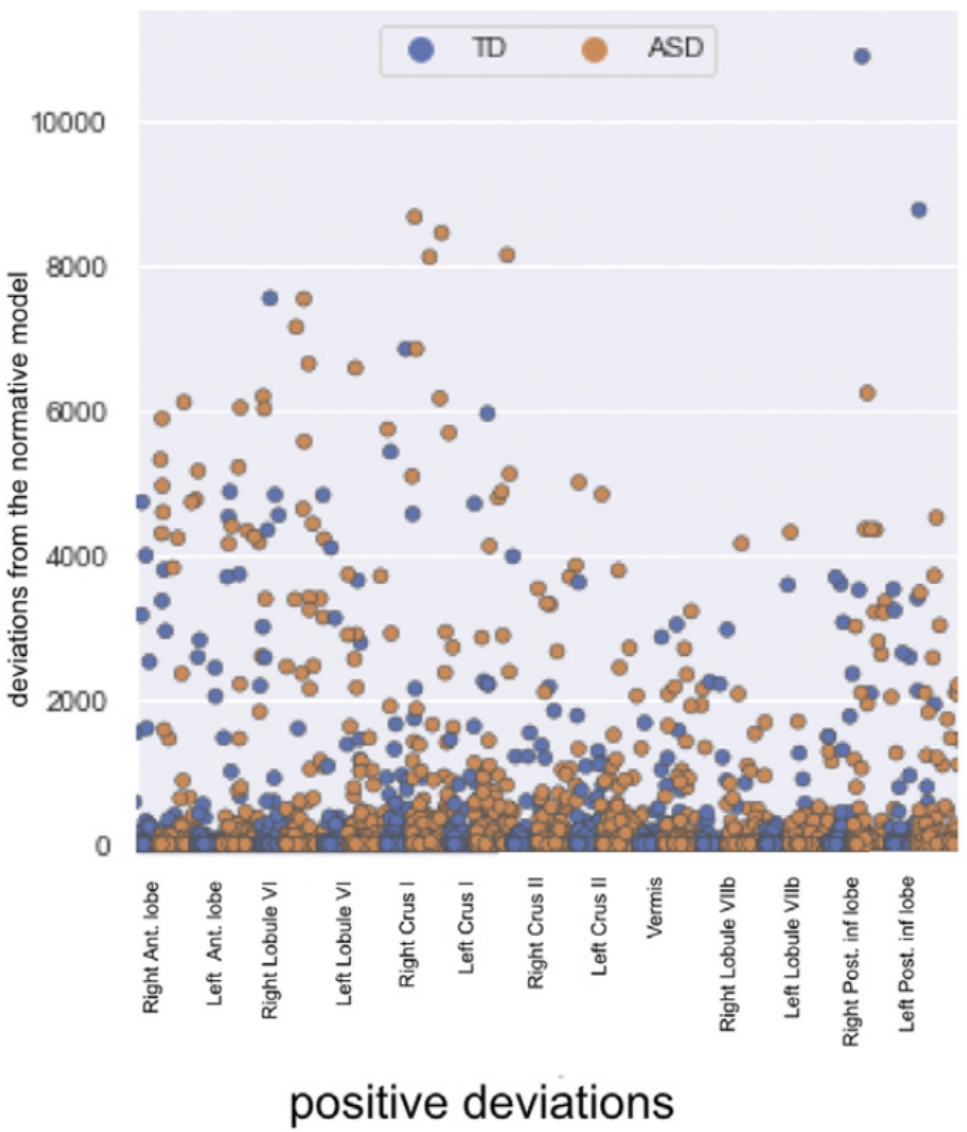

positive deviations

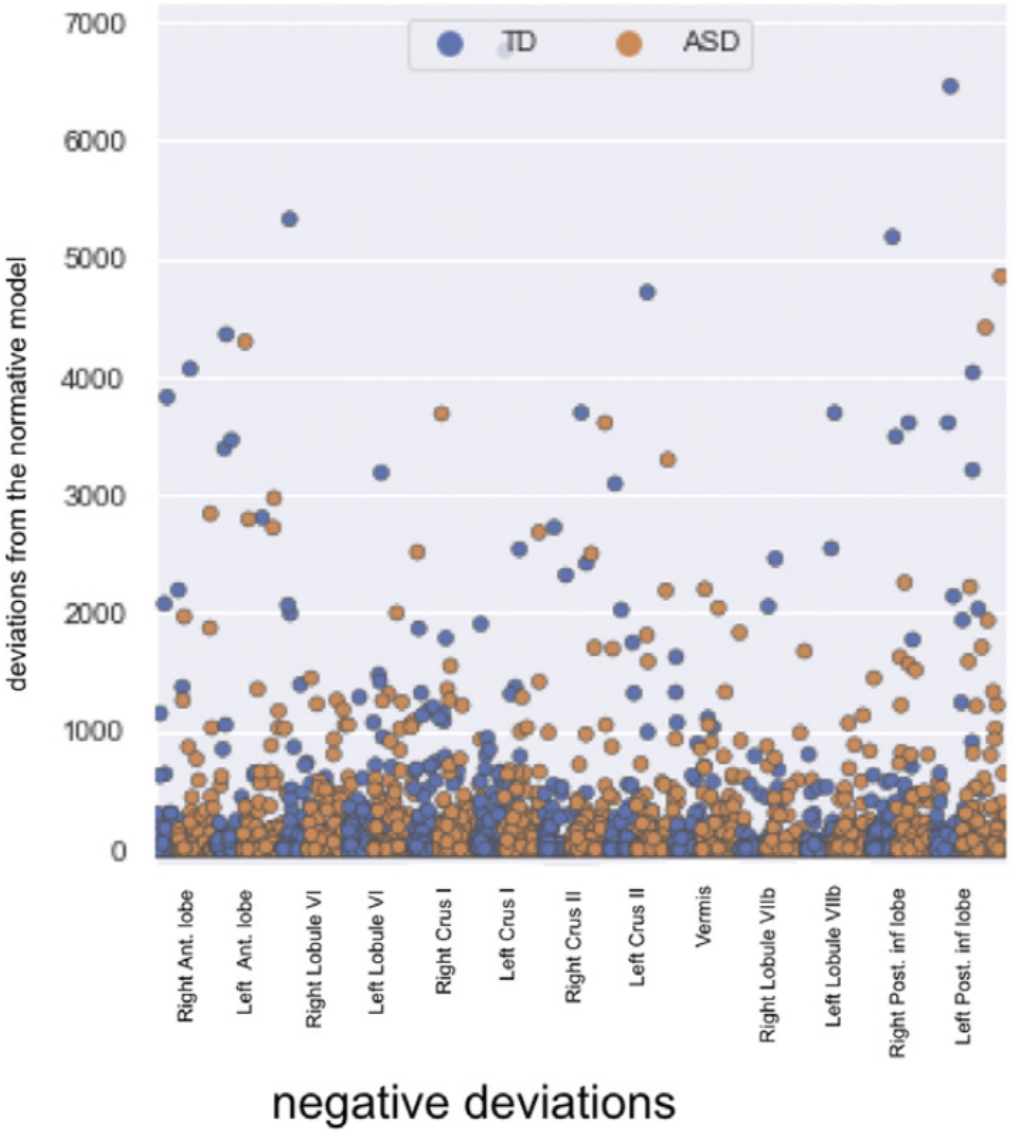

negative deviations

Image	Comment

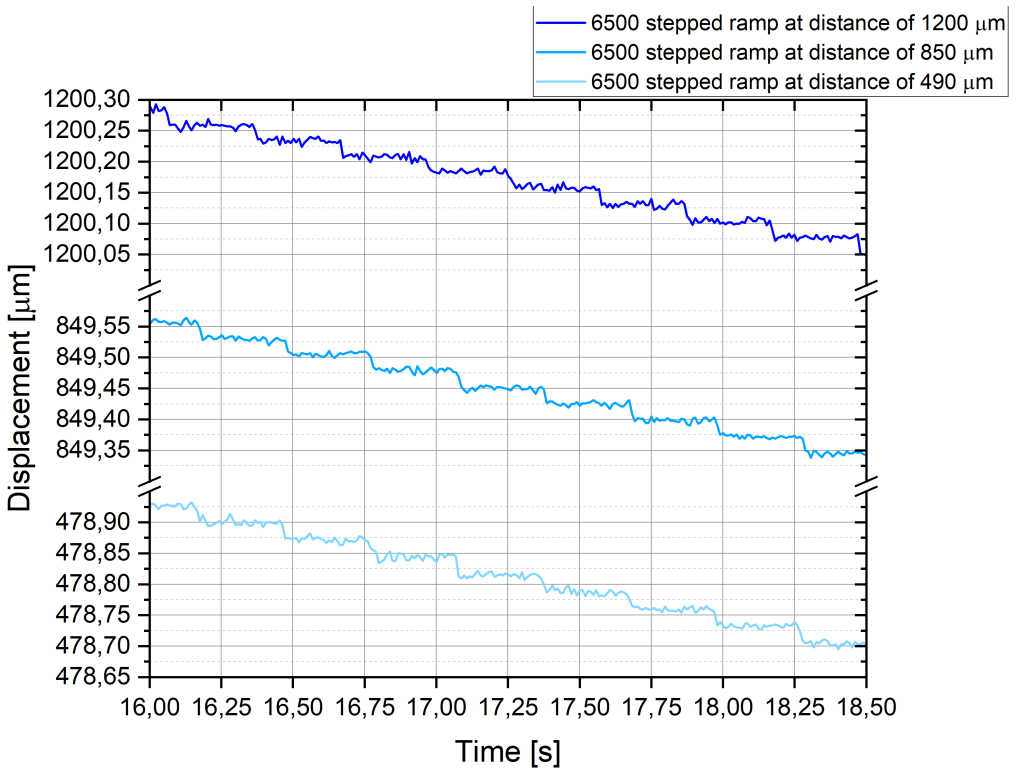

Image	Comment

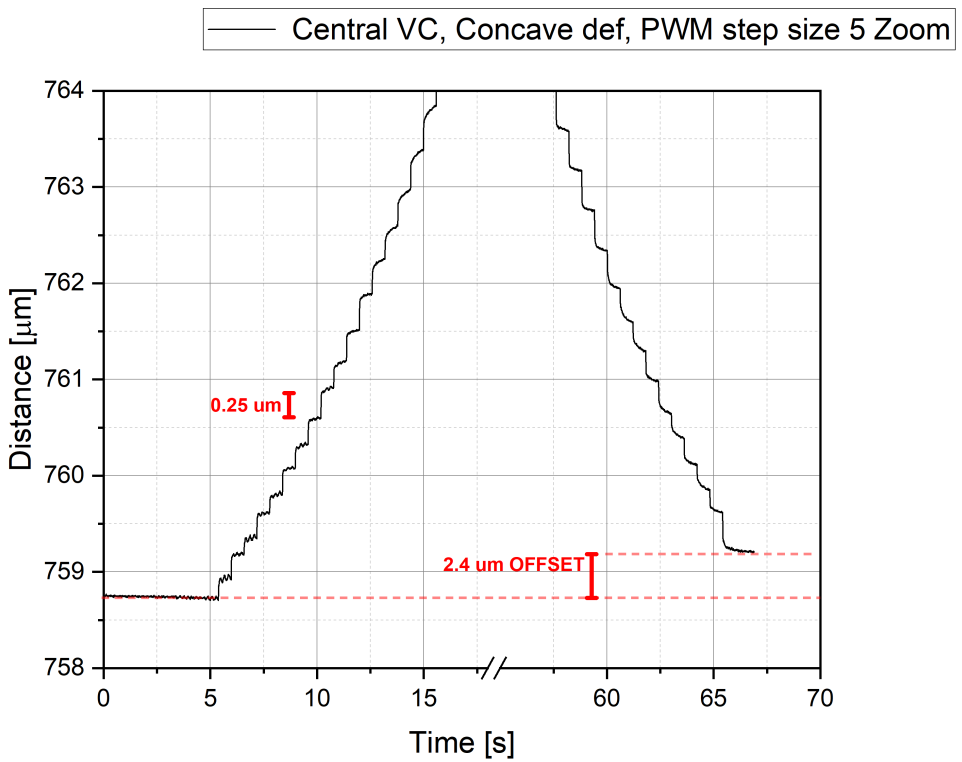

Image	Comment

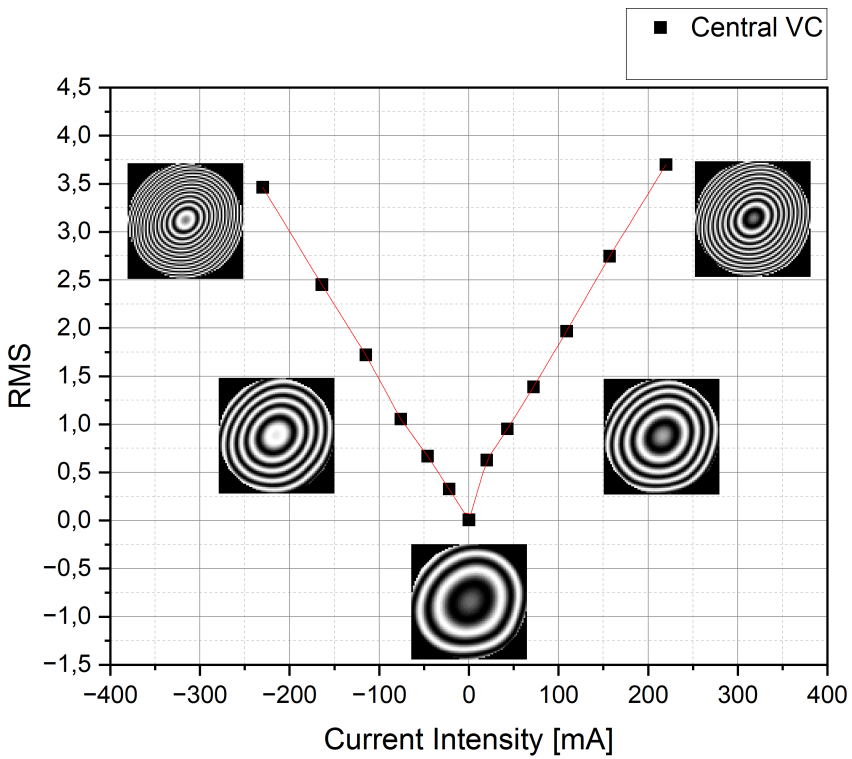

Image | Comment

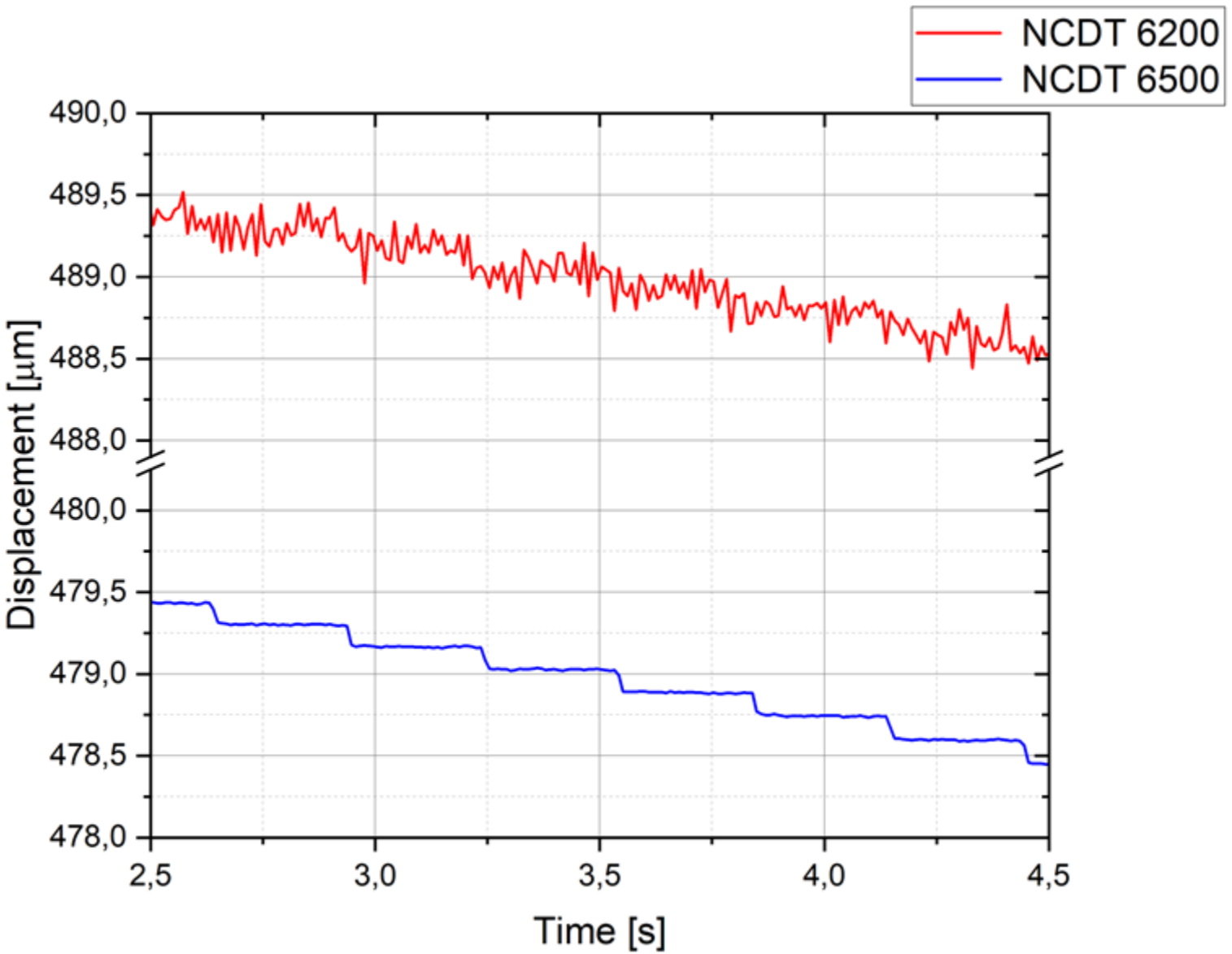

Image	Comment

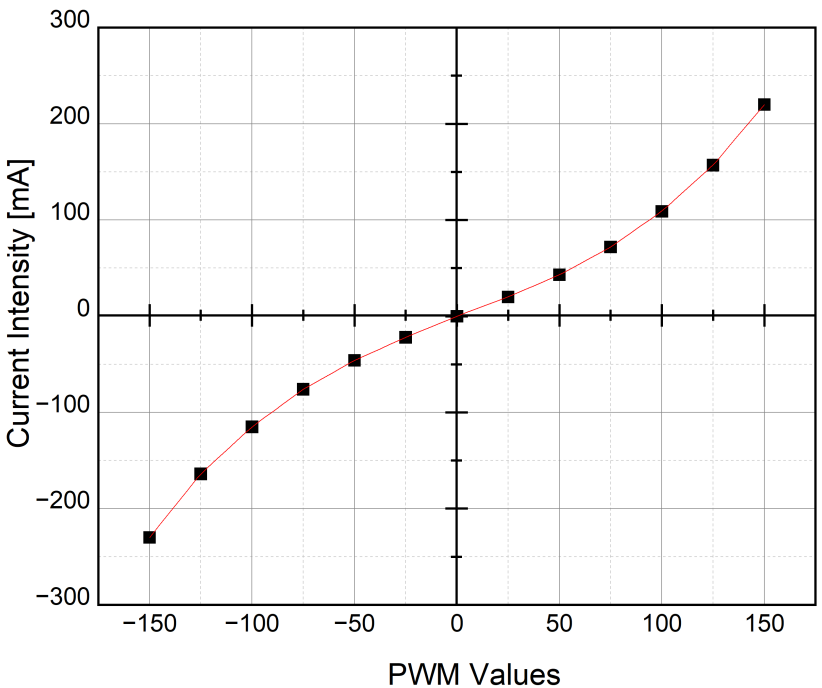

Image | Comment

(a)

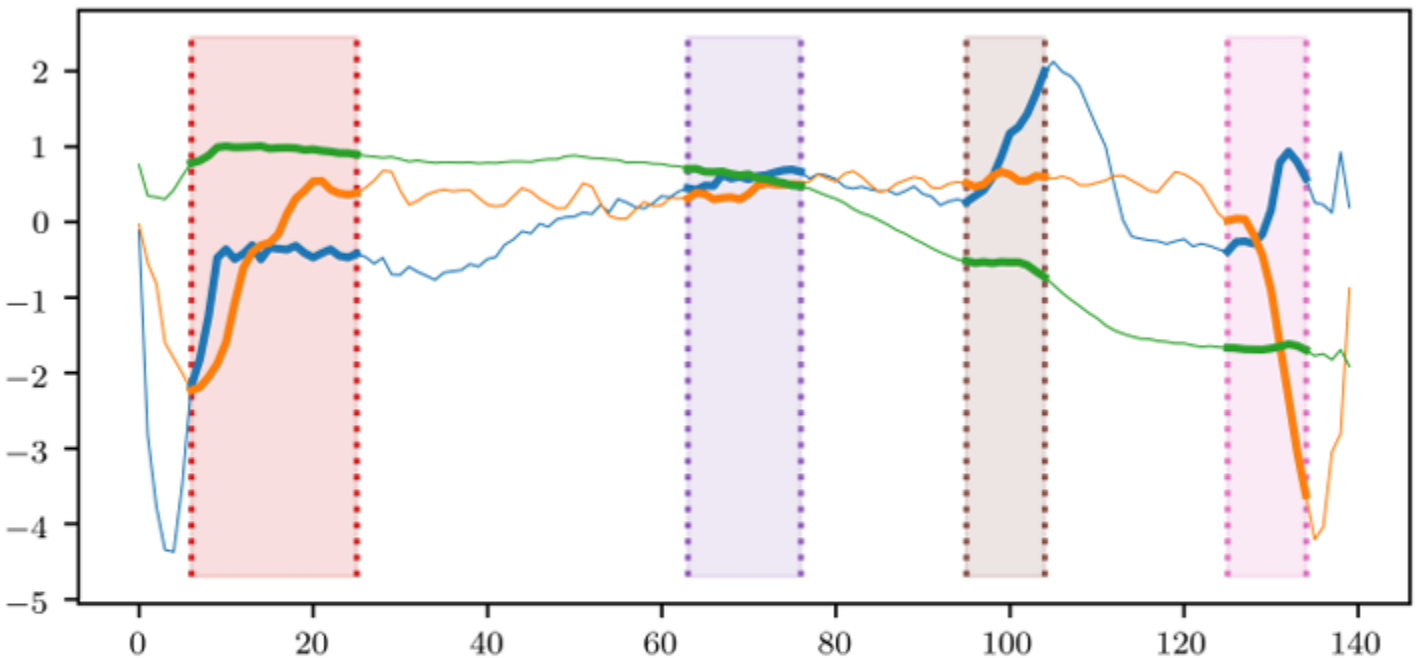

(b)

	Interval 1			Interval 2			Interval 3			Interval 4		
	Mean	SD	Slope	Mean	SD	Slope	Mean	SD	Slope	Mean	SD	Slope
Time series 1	-0.61	0.504	0.052	0.58	0.086	0.02	1.004	0.572	0.197	0.189	0.504	0.156
Time series 2	-0.467	0.977	0.158	0.403	0.084	0.017	0.568	0.061	0.011	-1.204	1.305	-0.431
Time series 3	0.944	0.061	0.002	0.604	0.075	-0.018	-0.57	0.065	-0.017	-1.671	0.024	0.003

Image | Comment

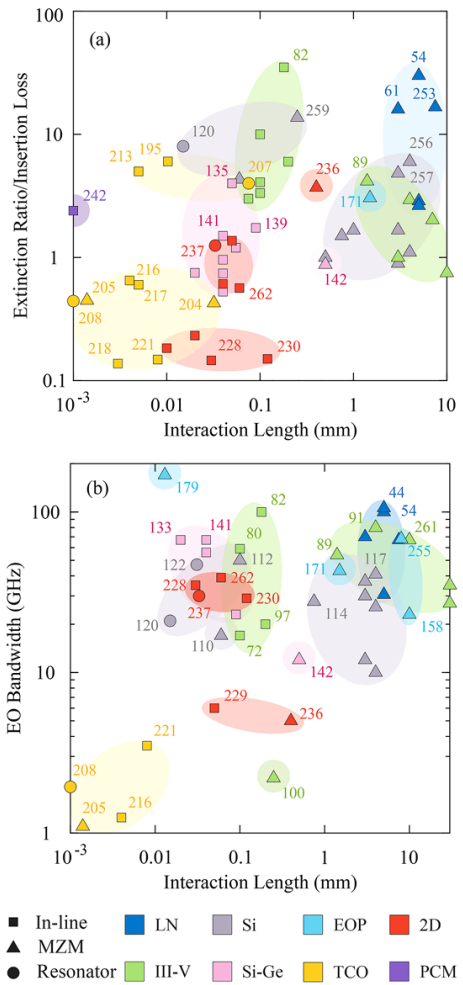

FIG. 19. Comparative assessment on the level of component. Performance metrics of demonstrated EO amplitude modulators employing in-line, MZI, or resonant configurations. (a) Ratio between the (static) ER and IL and (b) EO bandwidth, both as a function of the interaction length between the guided wave and the configurable material. Characteristic references are included as well.

Image	Comment

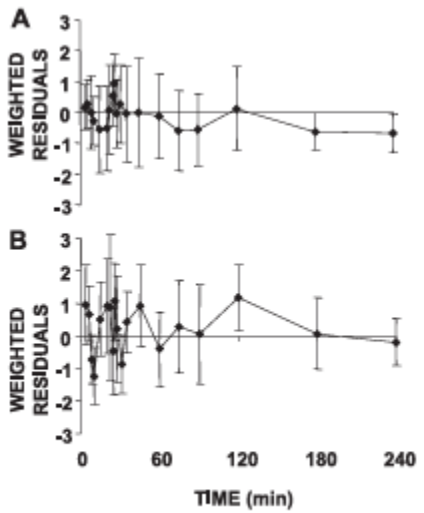

Fig. 4. Weighted residuals (means ± SD in 20 normal subjects) of C-peptide (*A*) and insulin (*B*) minimal models.

Image | Comment

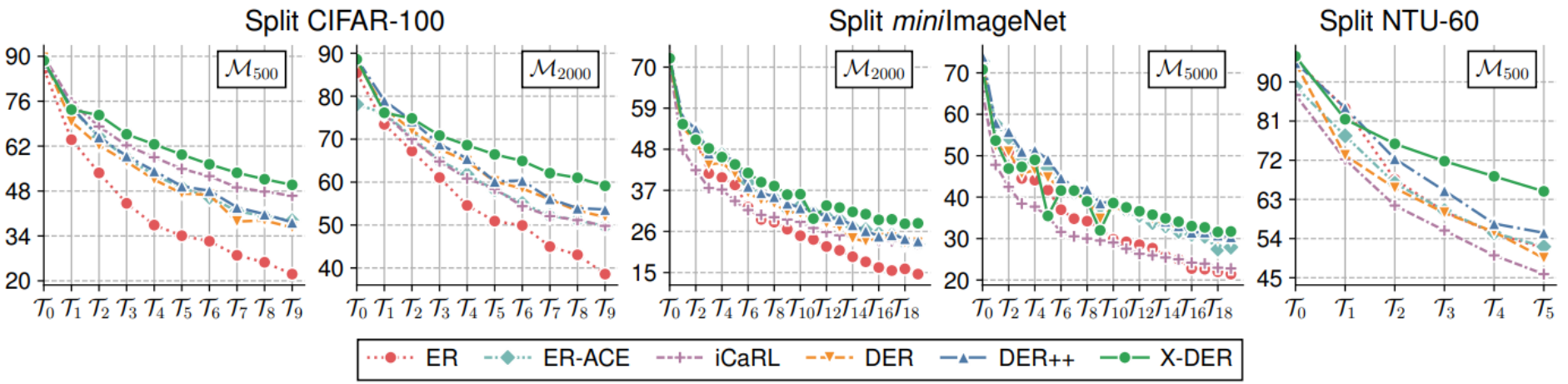

Fig. 6: For the experimental settings reported in Tab. 1, the trend of the average test-set accuracy on the observed tasks.

Image	Comment

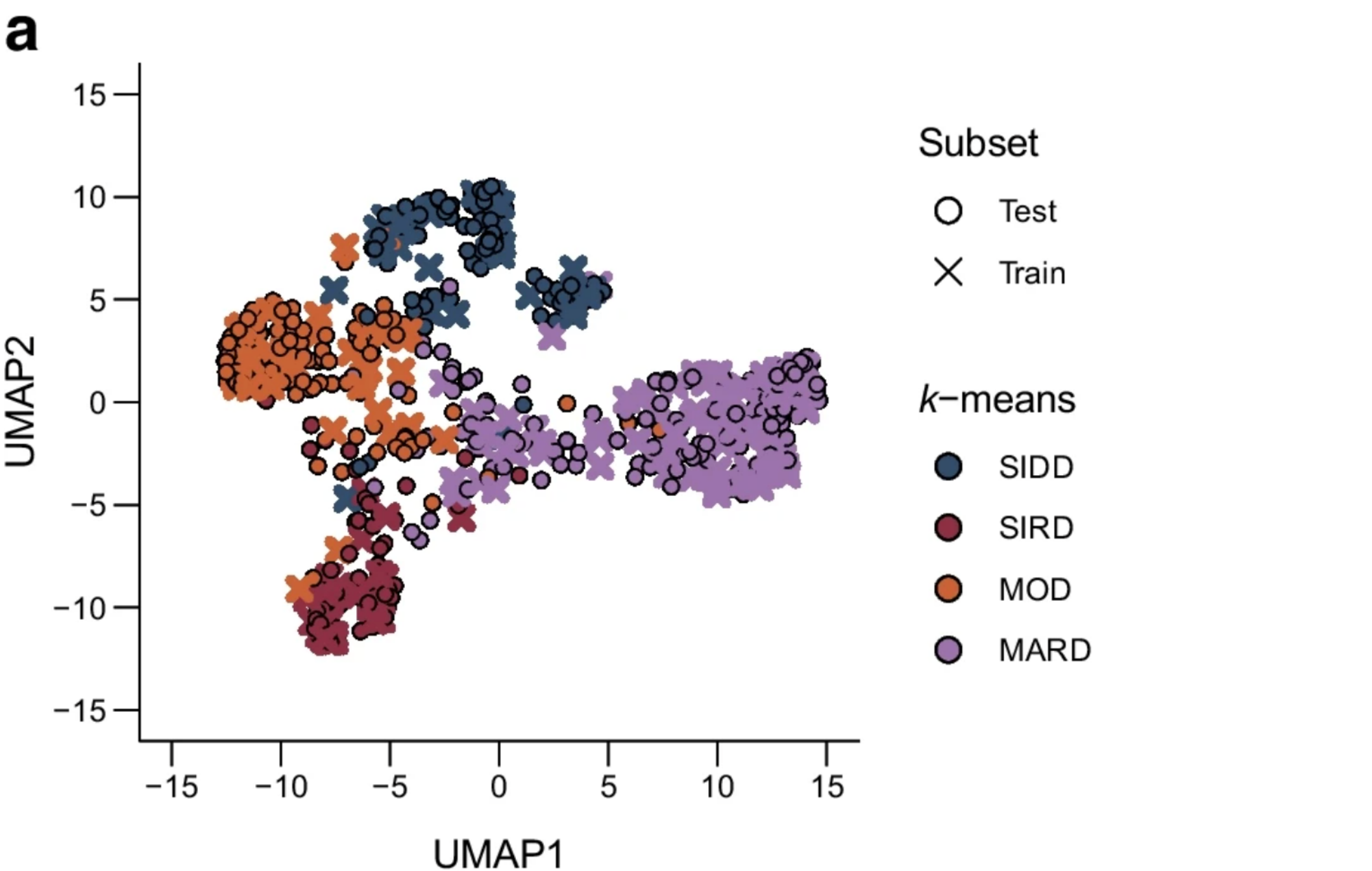
a
15
10
5
0
−5
−10
−15
UMAP2
−15
−10
−5
0
5
10
15
UMAP1
Subset
Test
Train
k−means
SIDD
SIRD
MOD
MARD

Image | Comment

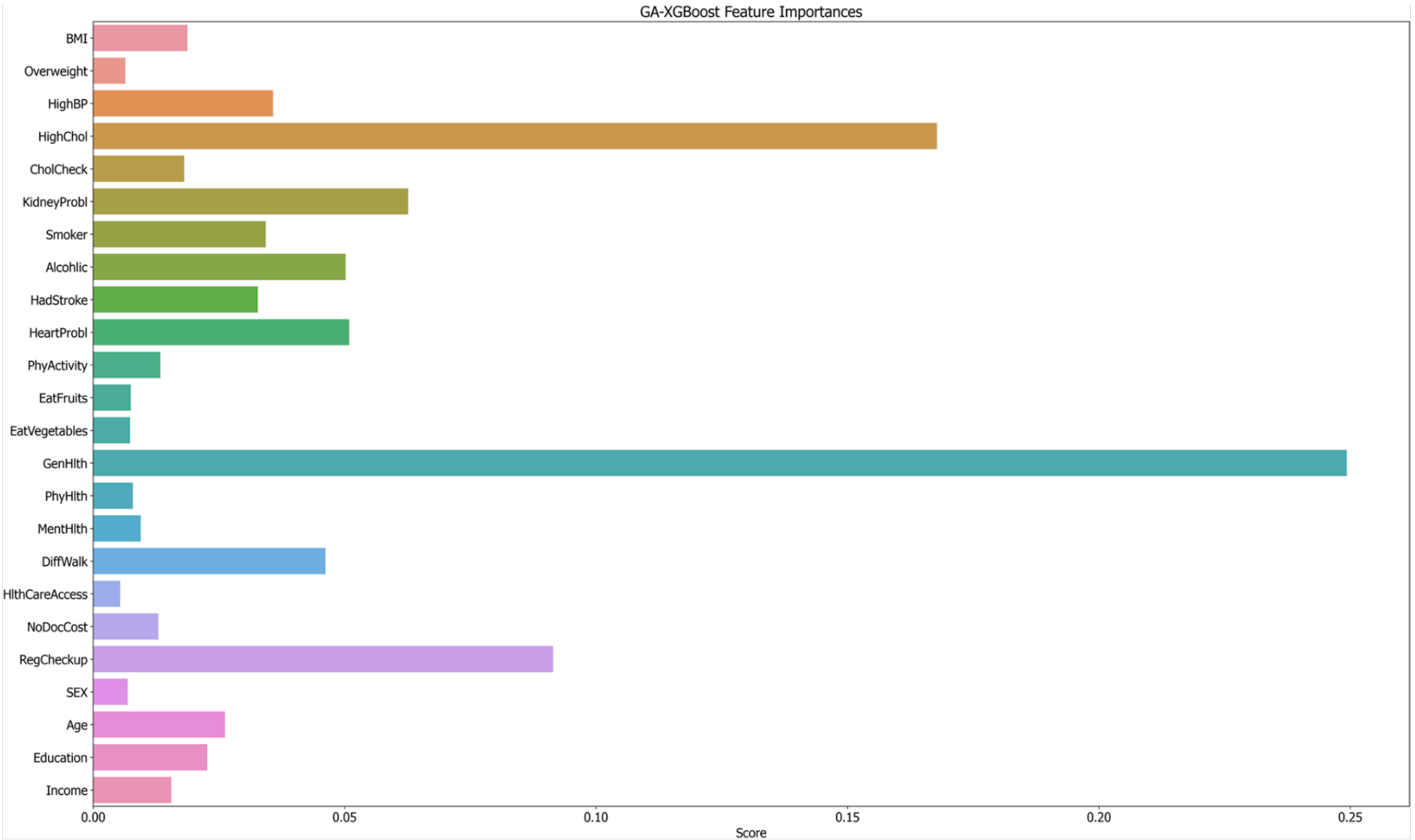

Image | Comment | Further comments

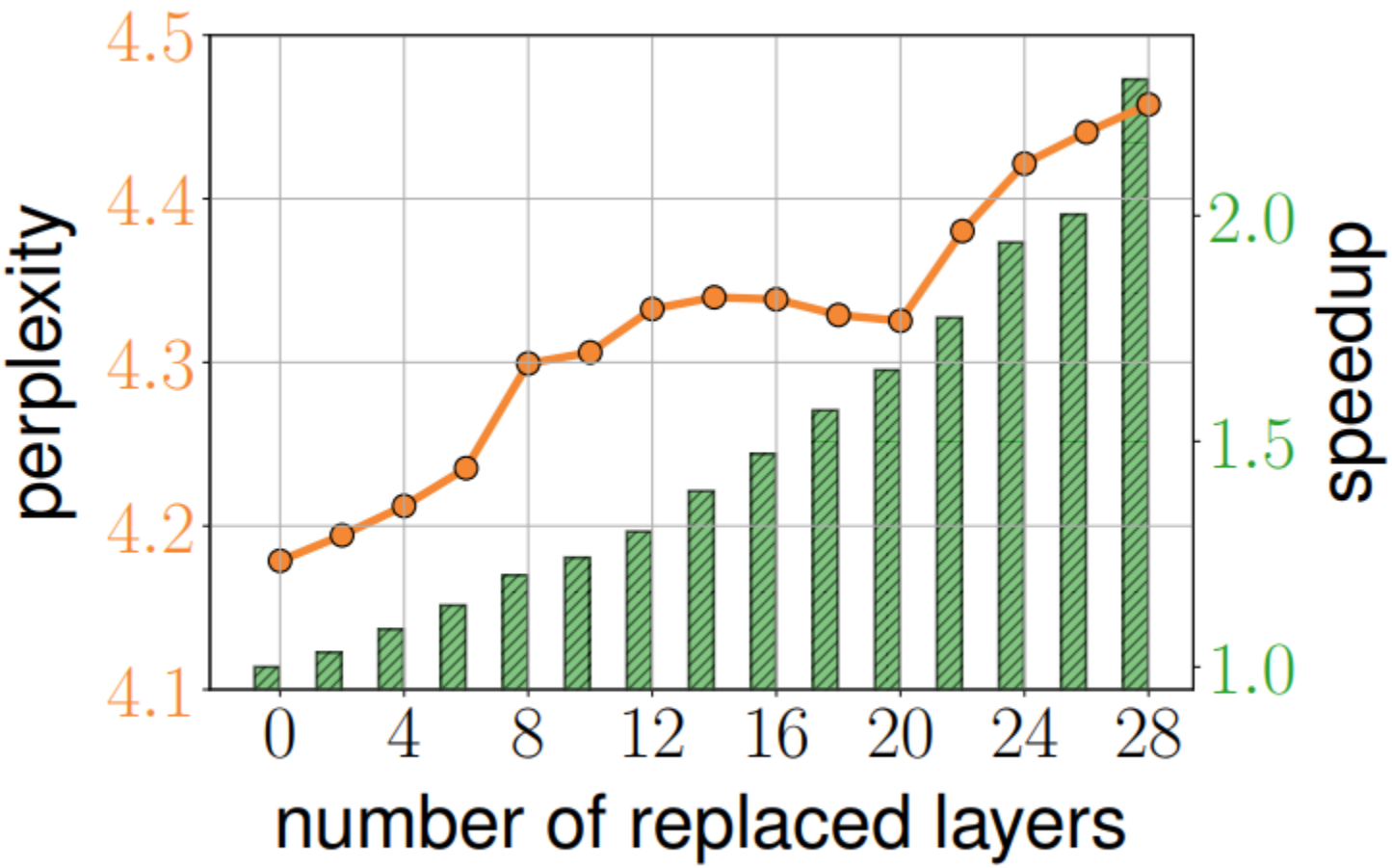

(a) chatglm3-6b-32k

Image	Comment

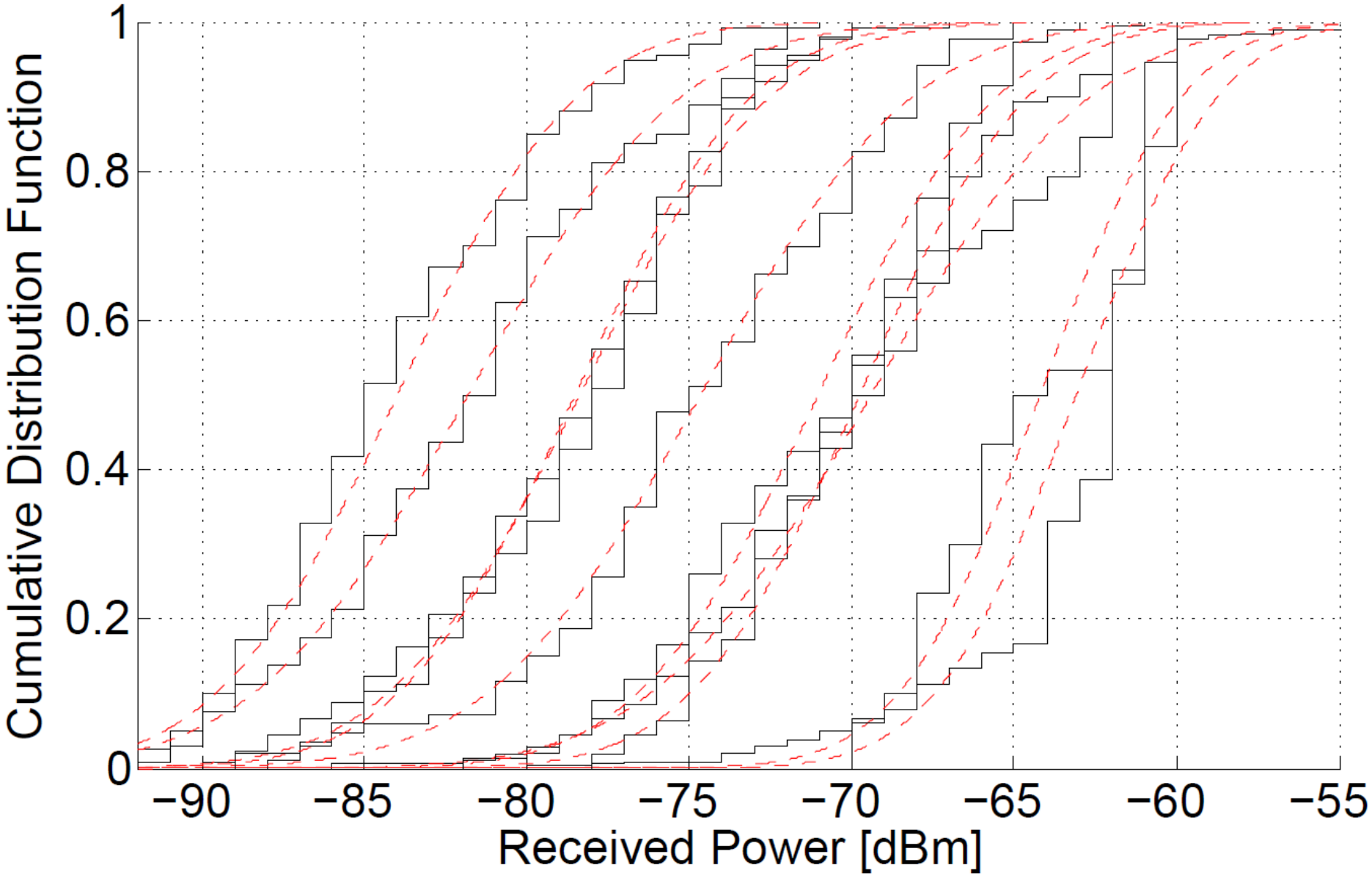
Cumulative Distribution Function
1
0.8
0.6
0.4
0.2
0
−90
−85
−80
−75
−70
−65
−60
−55
Received Power [dBm]

Image | Comment

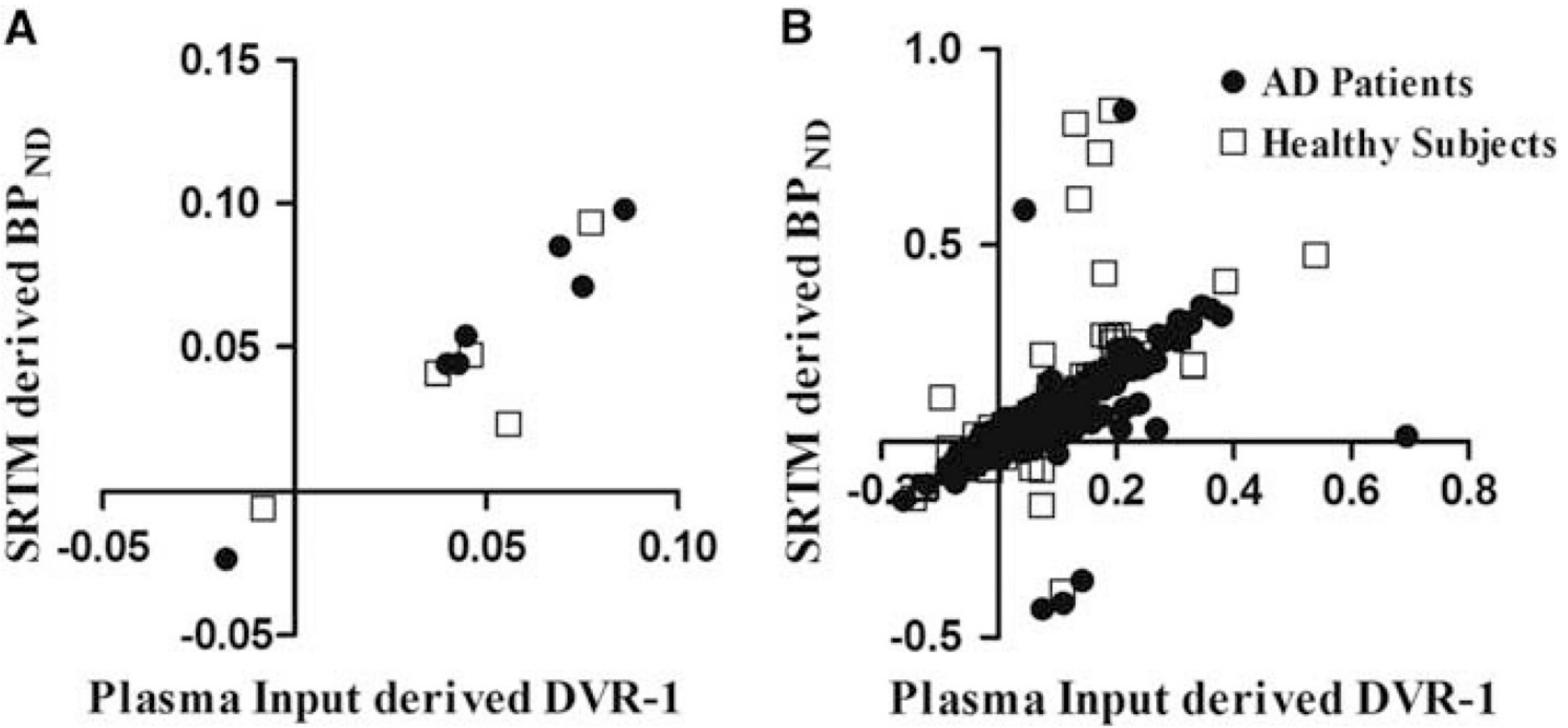

Image	Comment

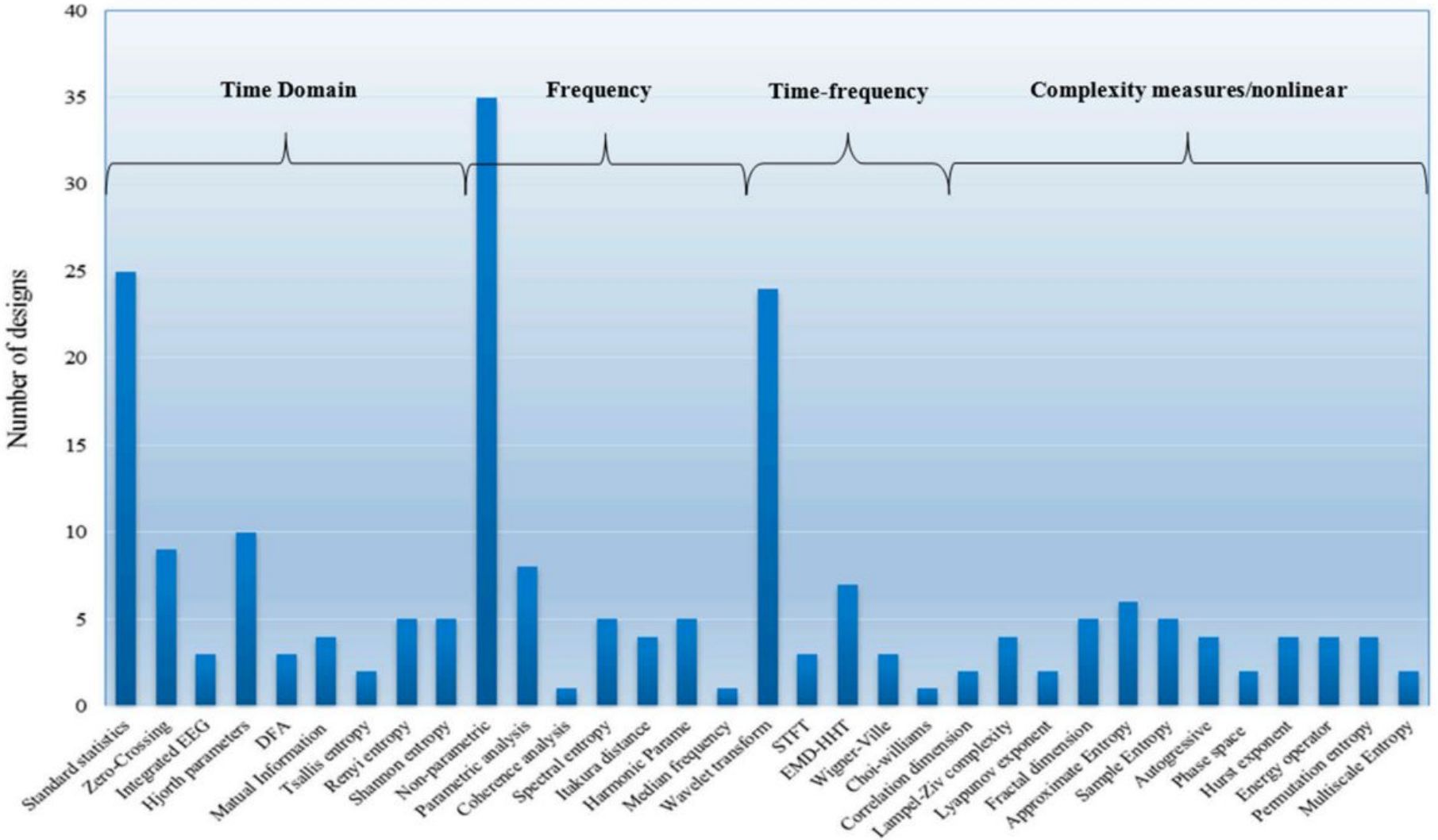

Figure 9. Feature extraction methods in ASSC schemes.

Image | Comment

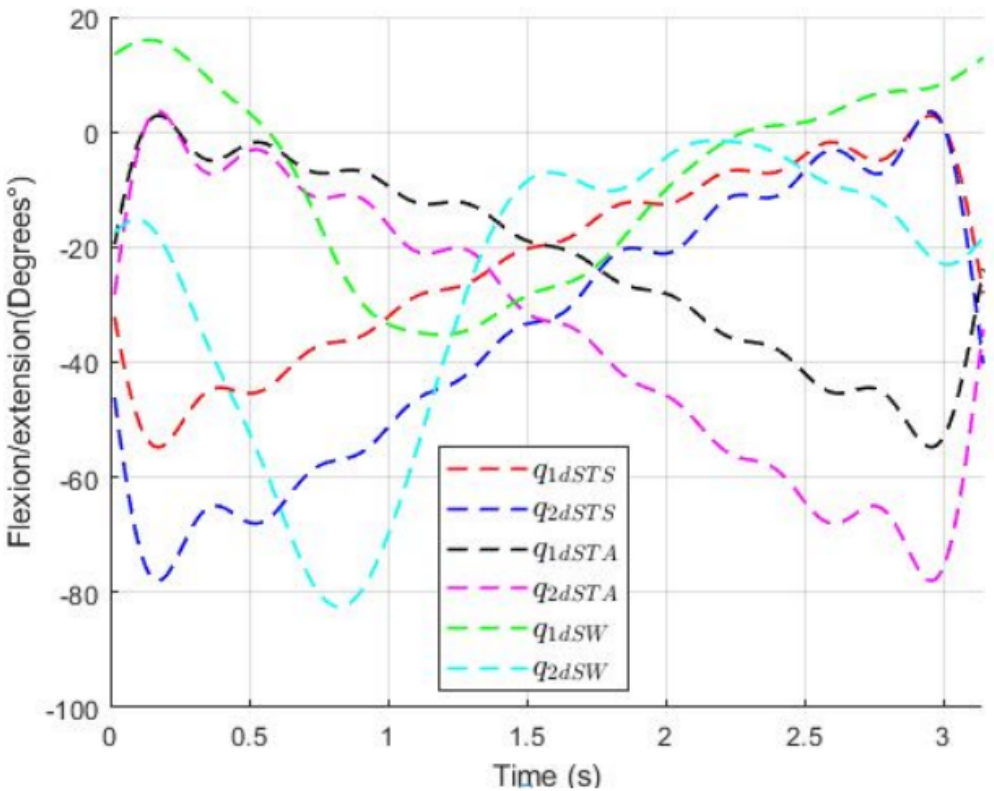

Figure 7. Motion trajectories for exoskeleton, sitting to standing $\boldsymbol{q_dSTS}$, standing to sitting $\boldsymbol{q_dSTA}$, and standing to walk $\boldsymbol{q_dSW}$, to the hip and knee joint denoted by q_{d1} and q_{d2}, respectively.

Image | Comment

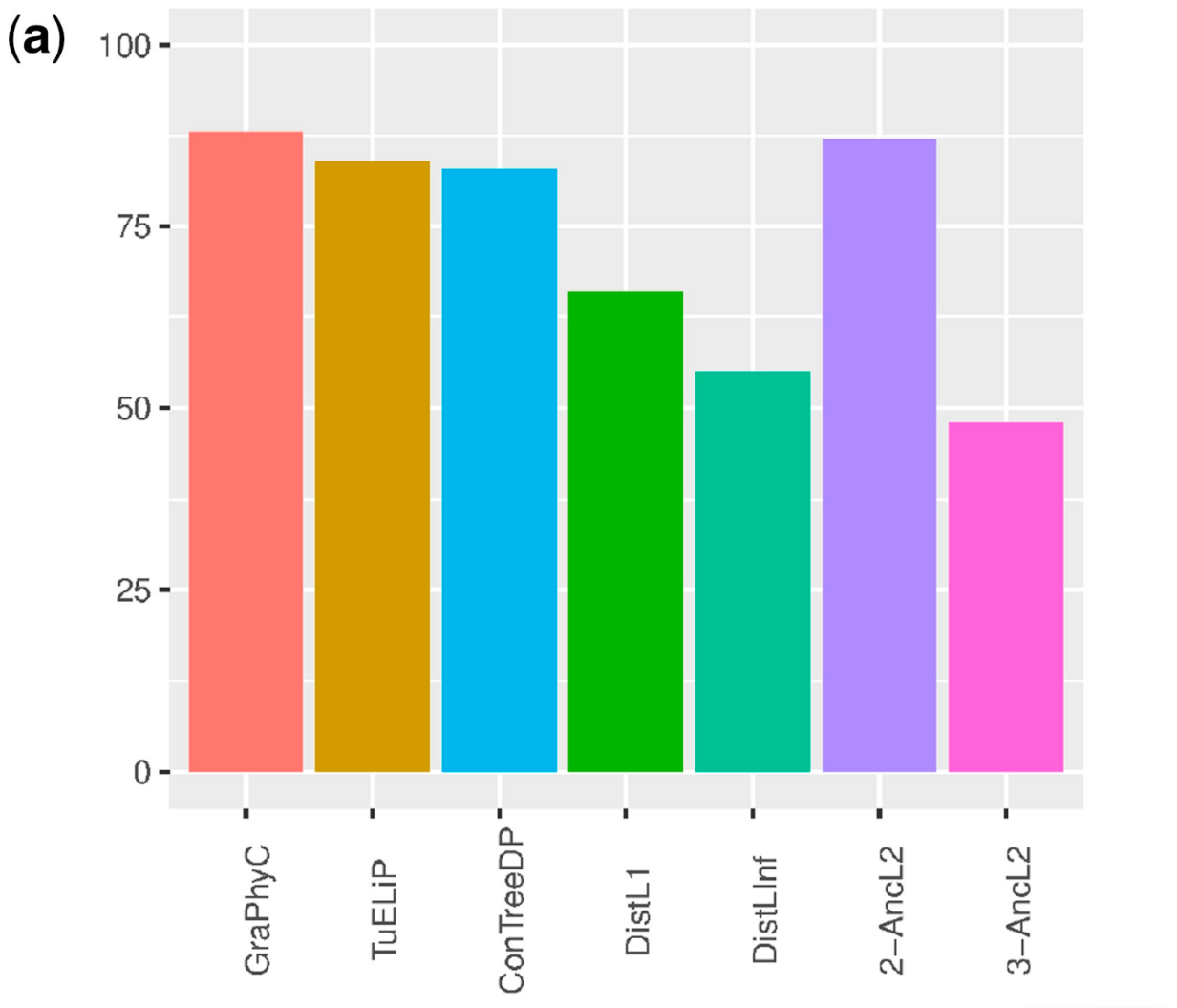

Image | Comment

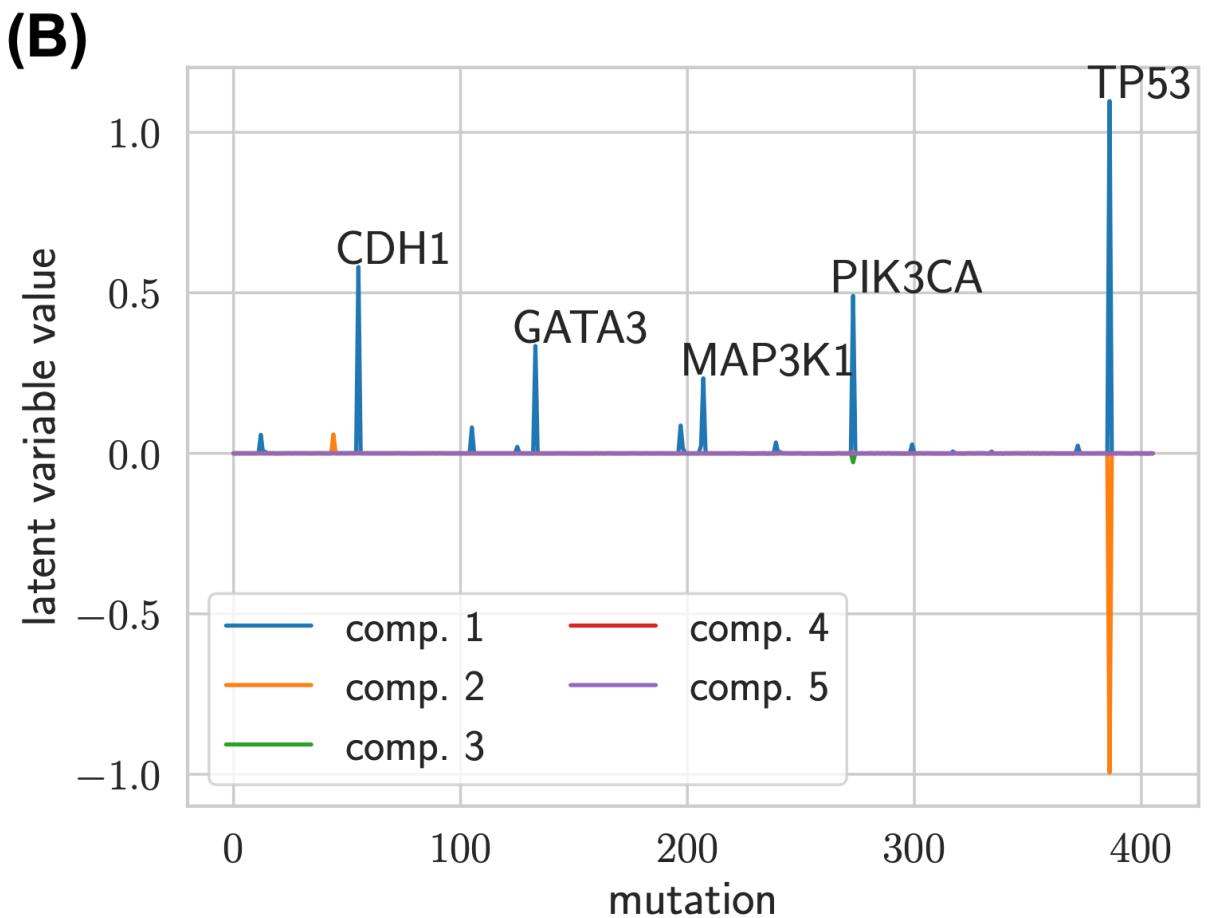

Image | Comment

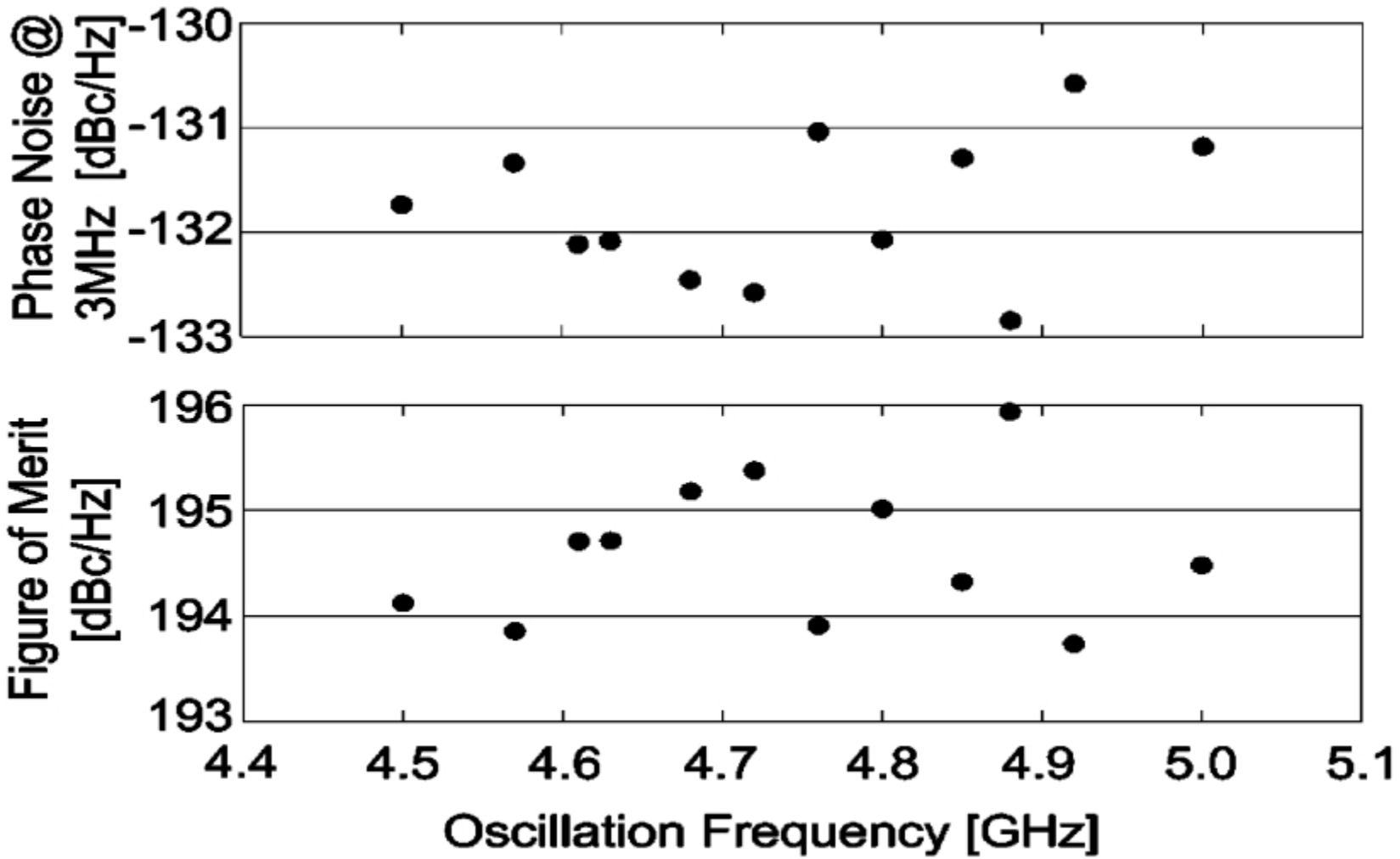

Image | Comment

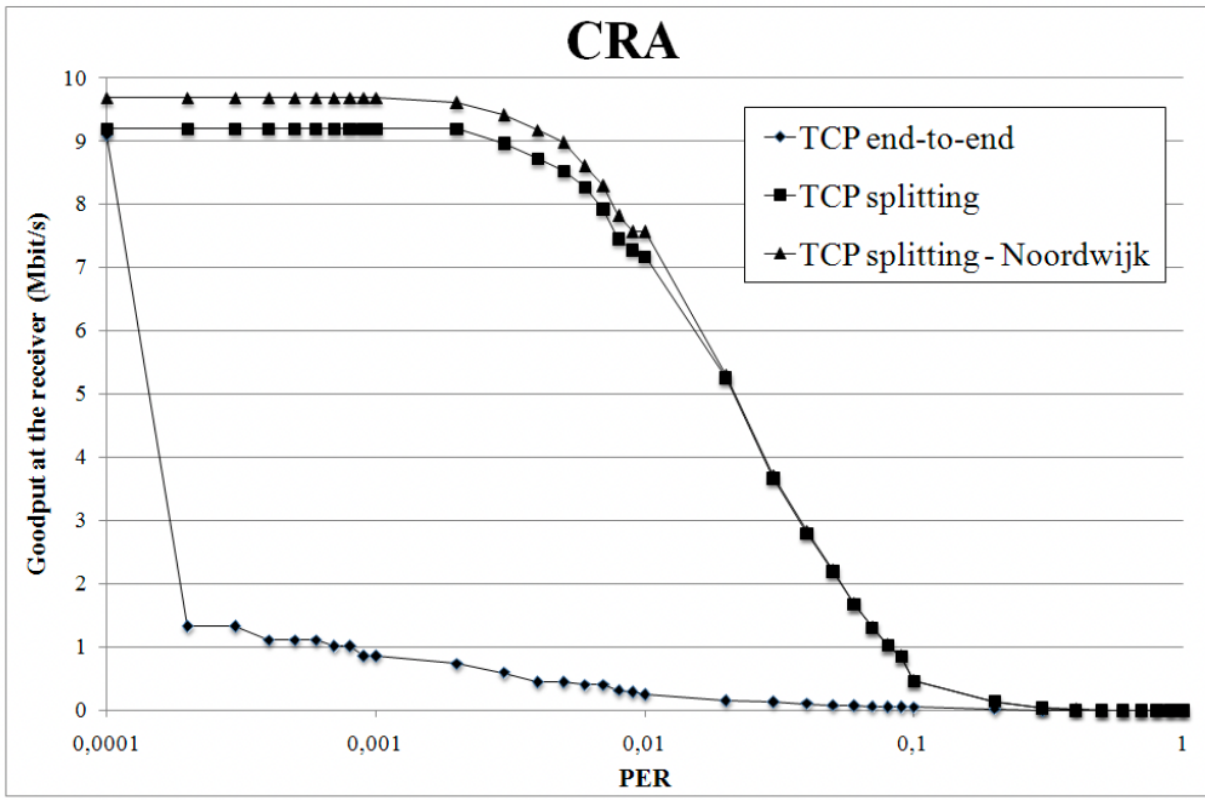

Figure 2: Goodput at the receiver vs. PER in the terrestrial wireless link; TCP transfer over satellite forward link; satellite return link access through CRA scheme

Image | Comment

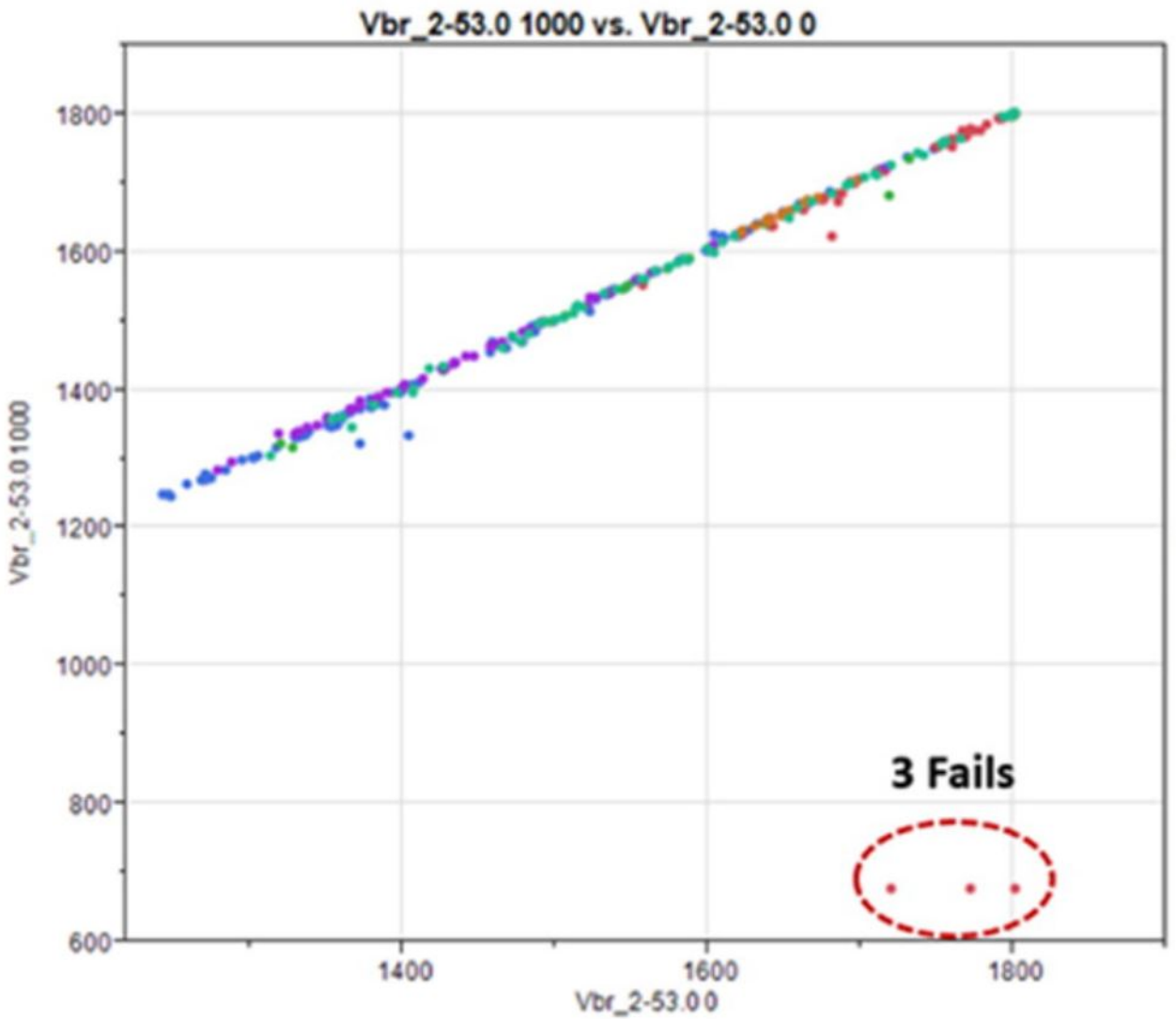

Image	Comment

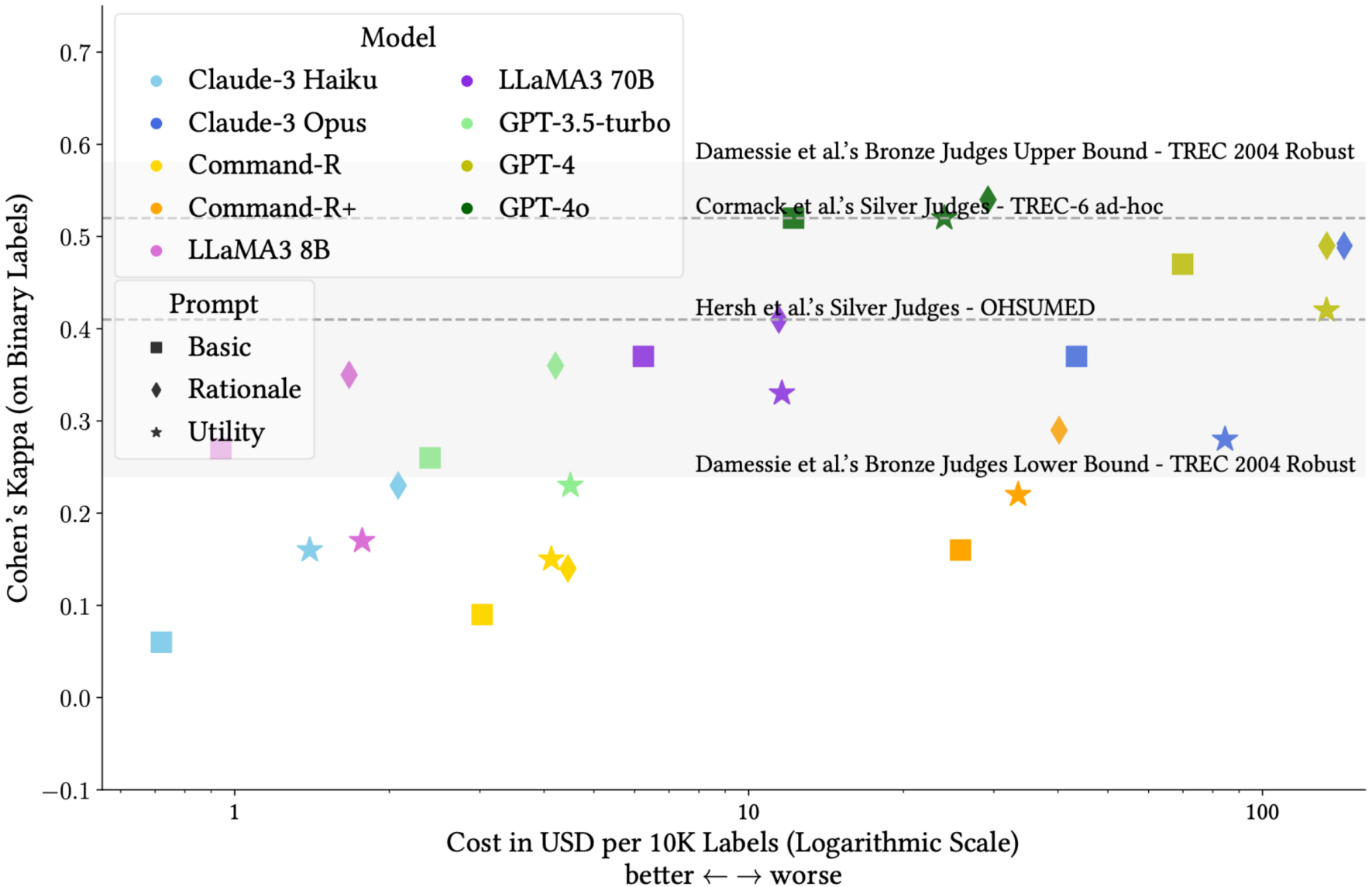
Model
Claude-3 Haiku
Claude-3 Opus
Command-R
Command-R+
LLaMA3 8B
LLaMA3 70B
GPT-3.5-turbo
GPT-4
GPT-4o
Prompt
Basic
Rationale
Utility
Damessie et al.'s Bronze Judges Upper Bound - TREC 2004 Robust
Cormack et al.'s Silver Judges - TREC-6 ad-hoc
Hersh et al.'s Silver Judges - OHSUMED
Damessie et al.'s Bronze Judges Lower Bound - TREC 2004 Robust
Cohen's Kappa (on Binary Labels)
0.7
0.6
0.5
0.4
0.3
0.2
0.1
0.0
−0.1
1
10
100
Cost in USD per 10K Labels (Logarithmic Scale)
better ← → worse

Image	Comment

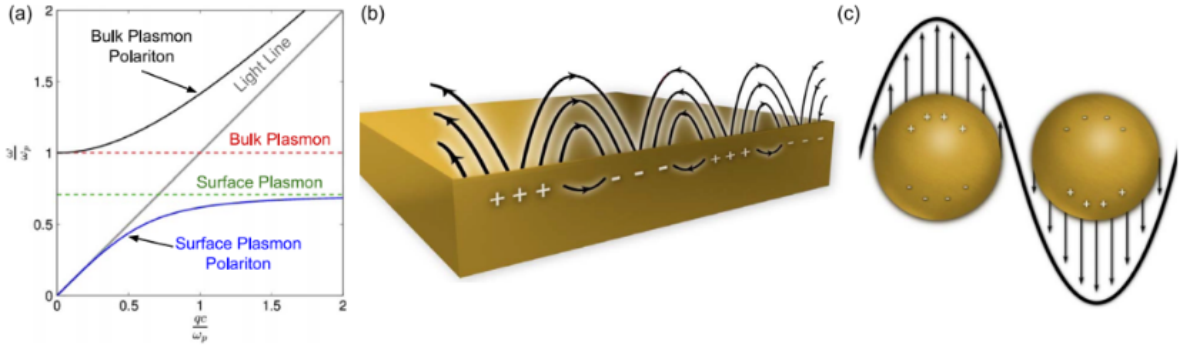

Fig. 1. *(a) Dispersion relations of plasmonic modes in a semi-infinite metal. (b) Surface plasmon polaritons at the interface between a metal and a dielectric showing the mixed character of a surface charge and an EM wave. (c) Localized surface plasmon in a metal nanoparticle.*

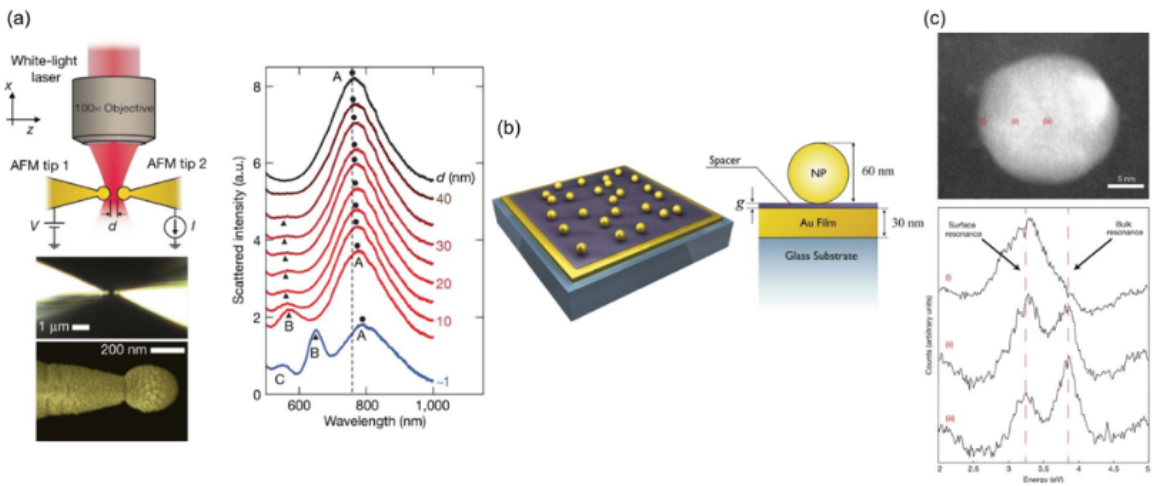

Fig. 2. *(a) Optical and electrical schema for measurements of plasmonic modes excited in two MNPs (coated tips) varying the gap distance d. The plasmonic resonances are labeled with letters A–C (reprinted by permission from [49]). (b) Example of a configuration where nonlocal effects are important, i.e., gold NPs on a gold film separated by a subnanometric layer (adapted from [50]). (c) Scanning transmission electron microscopy image of a 20-nm-diameter silver particle and the associated EELS data measured in different positions (reprinted by permission from [48]).*

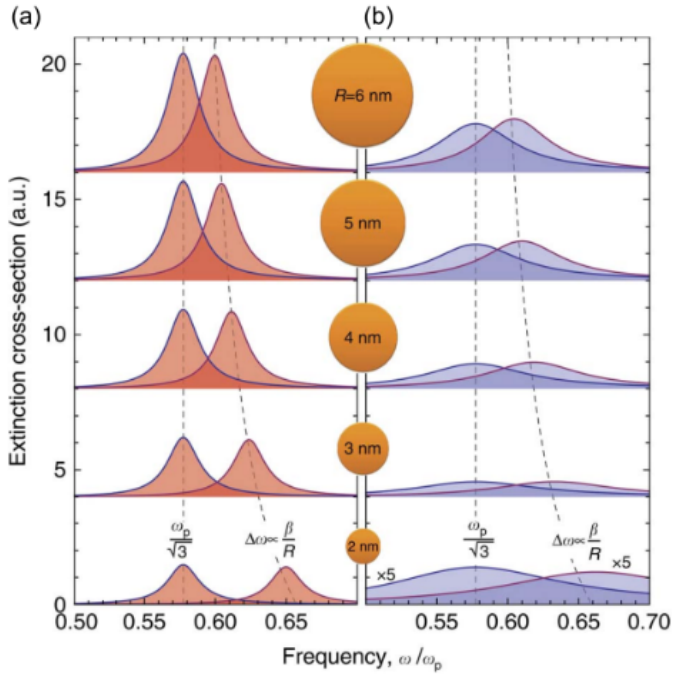

Fig. 3. *Extinction cross section for the localized plasmon resonance in a metal sphere with various radii. (a) Local Drude calculations compared with nonlocal hydrodynamic results. (b) The same as (a) but considering a phenomenological broadening in the local calculations and a diffusive term in the hydrodynamic model (reprinted by permission from [100]).*

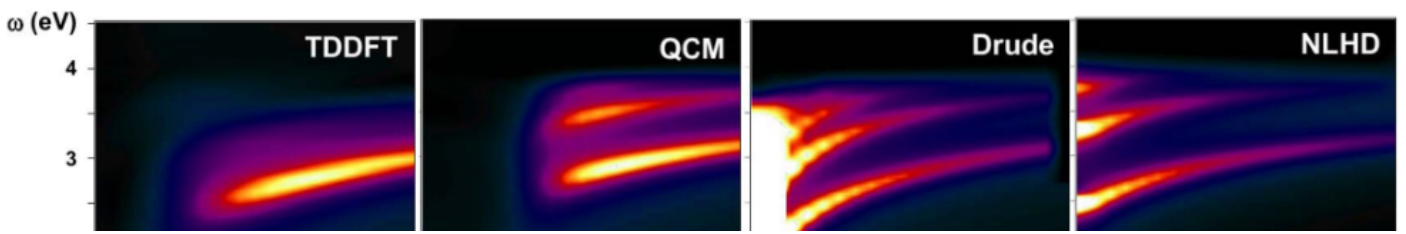

Image | Comment

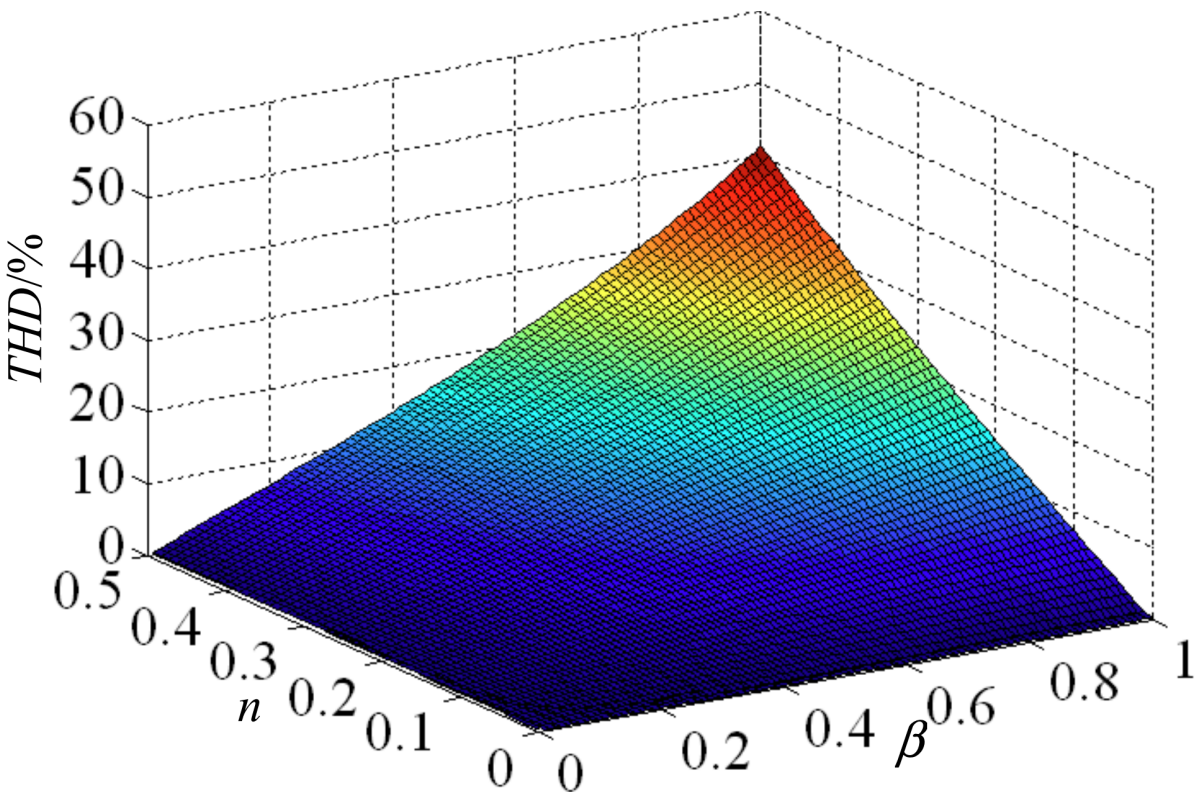

(a)

Image | Comment

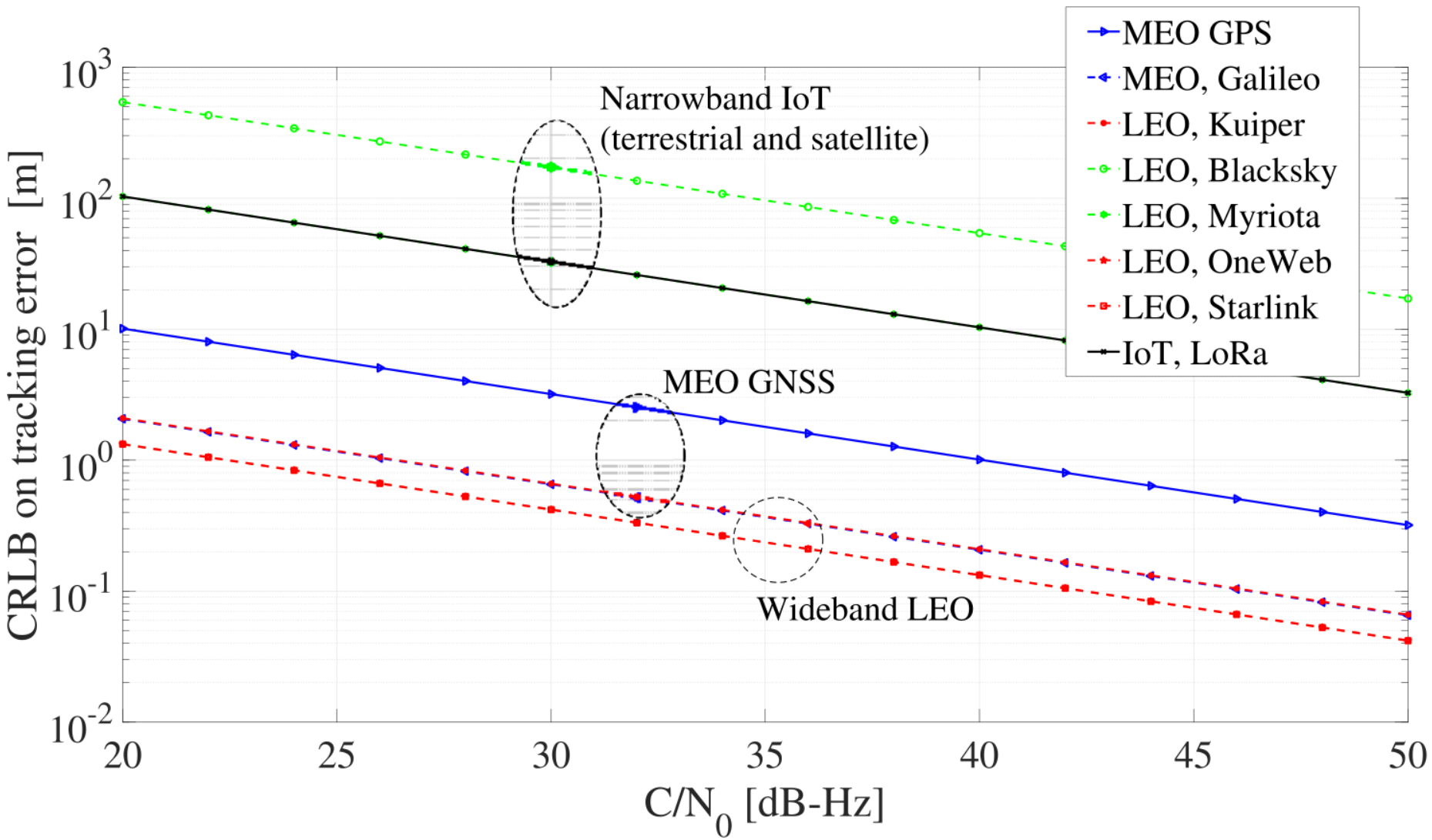

Image | Comment

standardized DALY rate of musculoskeletal disorders and SDI at the global and regional levels from 1990 and 2017, such that the burden of musculoskeletal disorders increased with SDI (Figure 5).

This study provides up-to-date musculoskeletal disorder prevalence, death, and DALY counts between 1990 and 2017, in addition to age-standardized rates across regional and

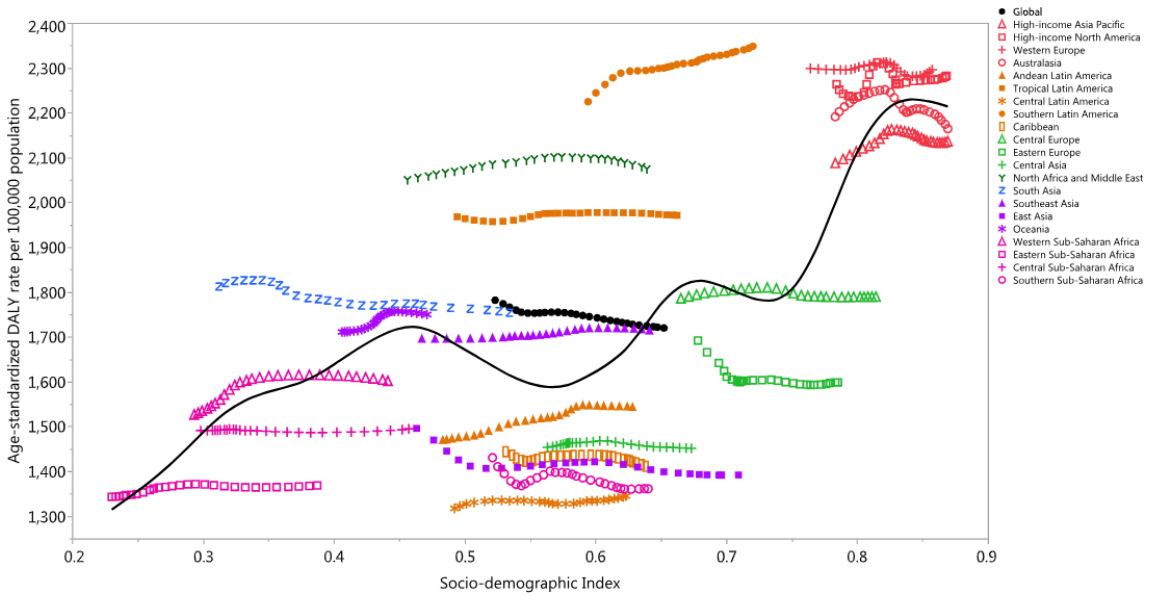

Figure 5. Age-standardized disability-adjusted life year (DALY) rates for musculoskeletal disorders for 21 Global Burden of Disease (GBD) regions according to Sociodemographic Index (SDI), 1990–2017 (generated from data available from http://ghdx.healthdata.org/gbd-results-tool). Black line indicates expected values in all locations based on SDI and disease rates. Twenty-eight points are plotted for each GBD region and show observed age-standardized DALY rates from 1990 to 2017 for that region. Color figure can be viewed in the online issue, which is available at http://onlinelibrary.wiley.com/doi/10.1002/art.41571/abstract.

Image | Comment

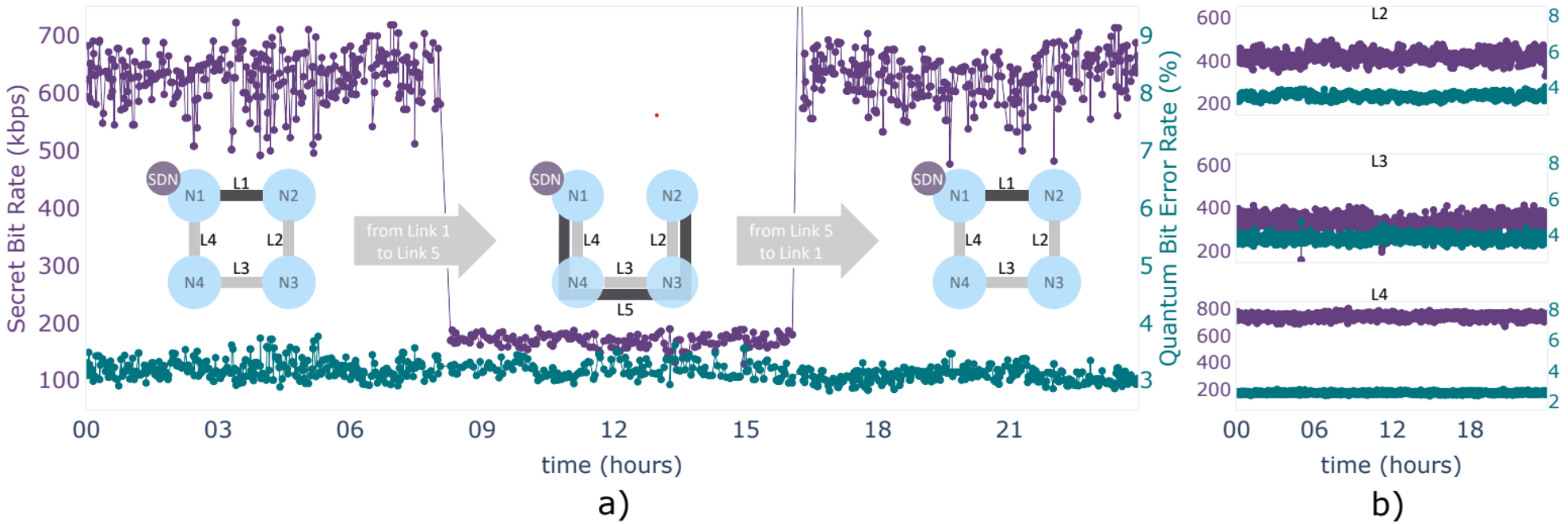

Fig. 3. Monitoring data acquired by the SDN Controller during 24 hours of operation. The secret bit rate (SBR) and quantum bit error rate (QBER) showed in purple and teal colors, respectively. a) shows the two switching operations performed back and forth from links L1 and L5. Due to L5's higher losses, a reduction in SBR is perceived. b) monitored data of links L2, L3 and L4.

Image | Comment

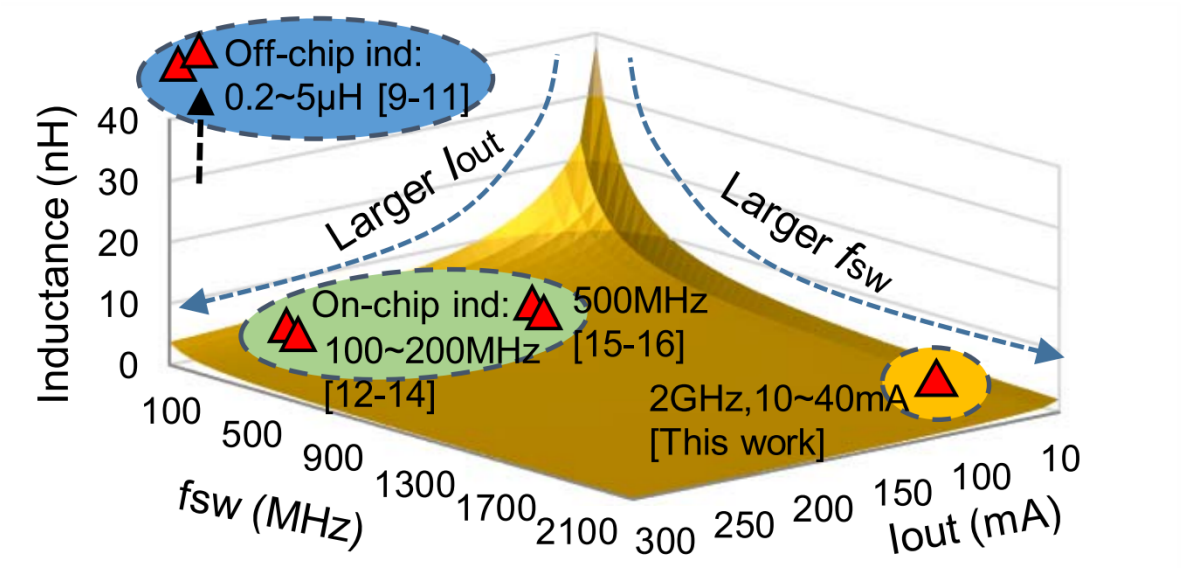

(b)

arameters. (b) Inductance versus switching frequency and load current for buck

Image	Comment

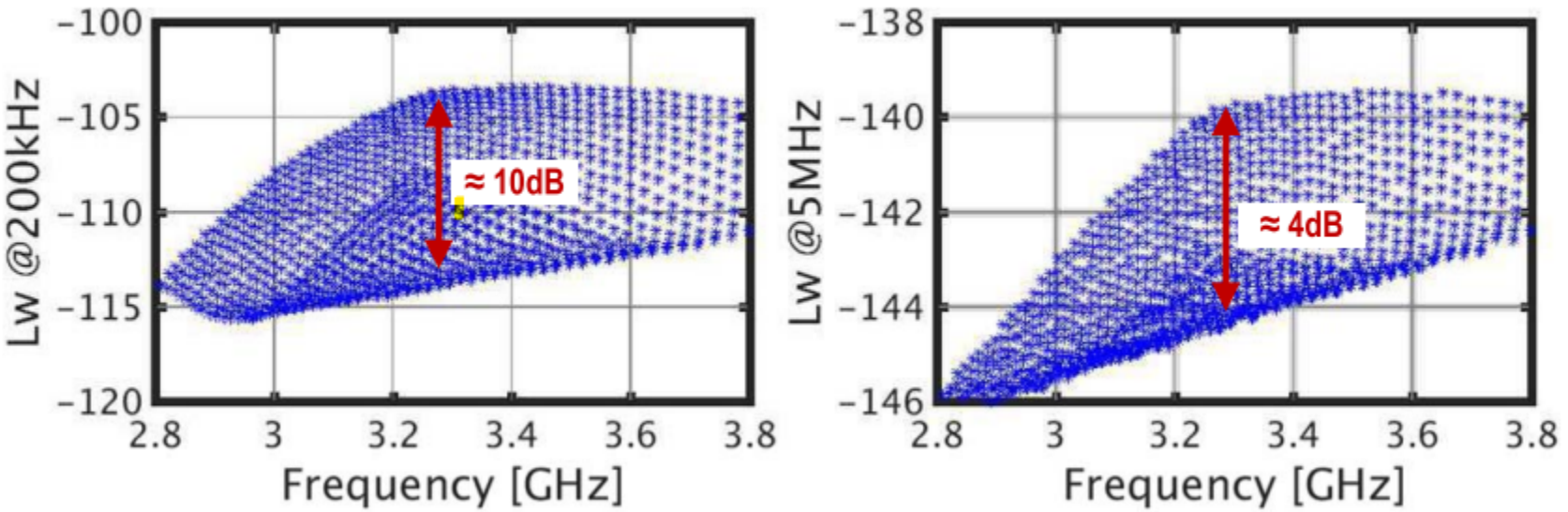

Image | Comment

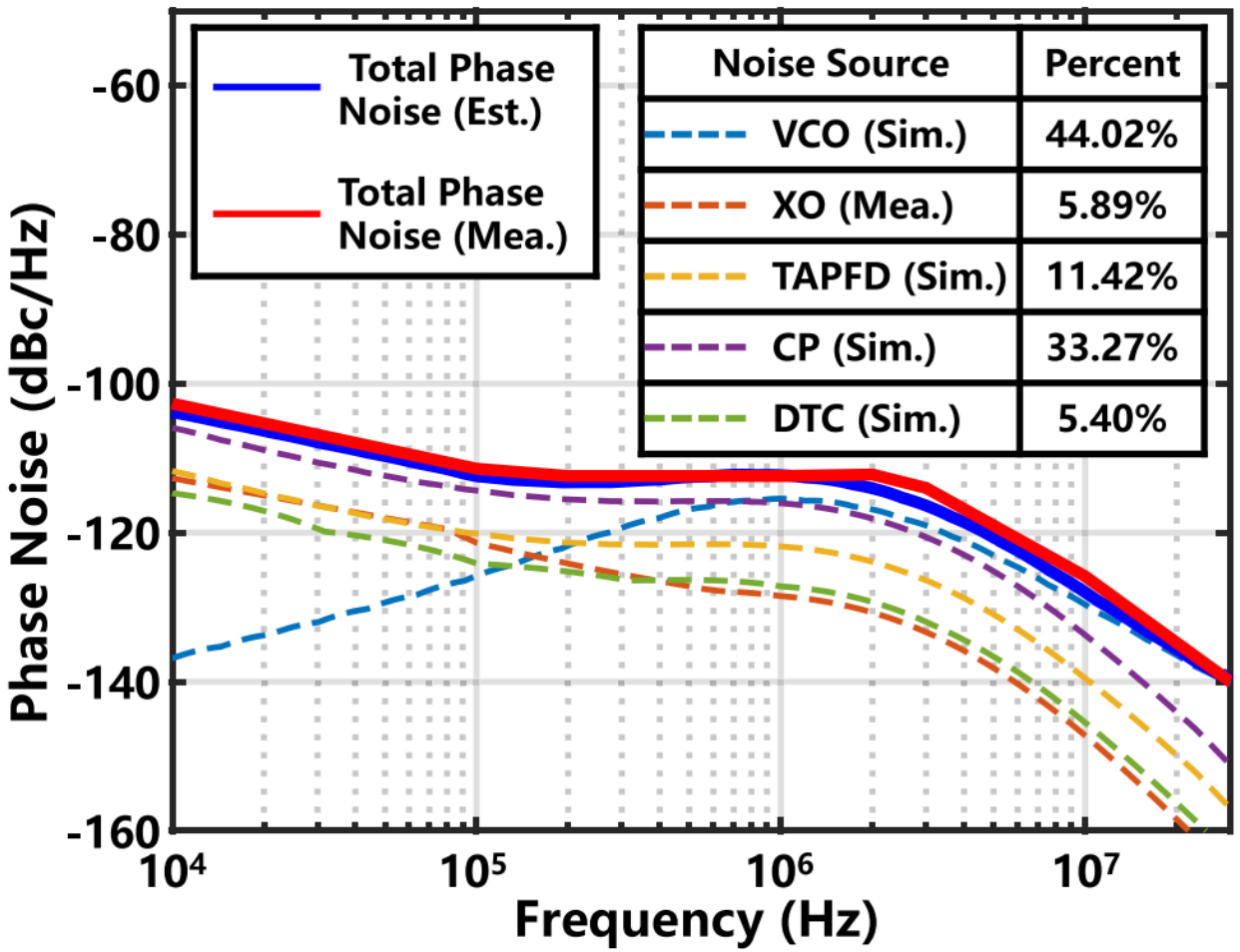

Image	Comment

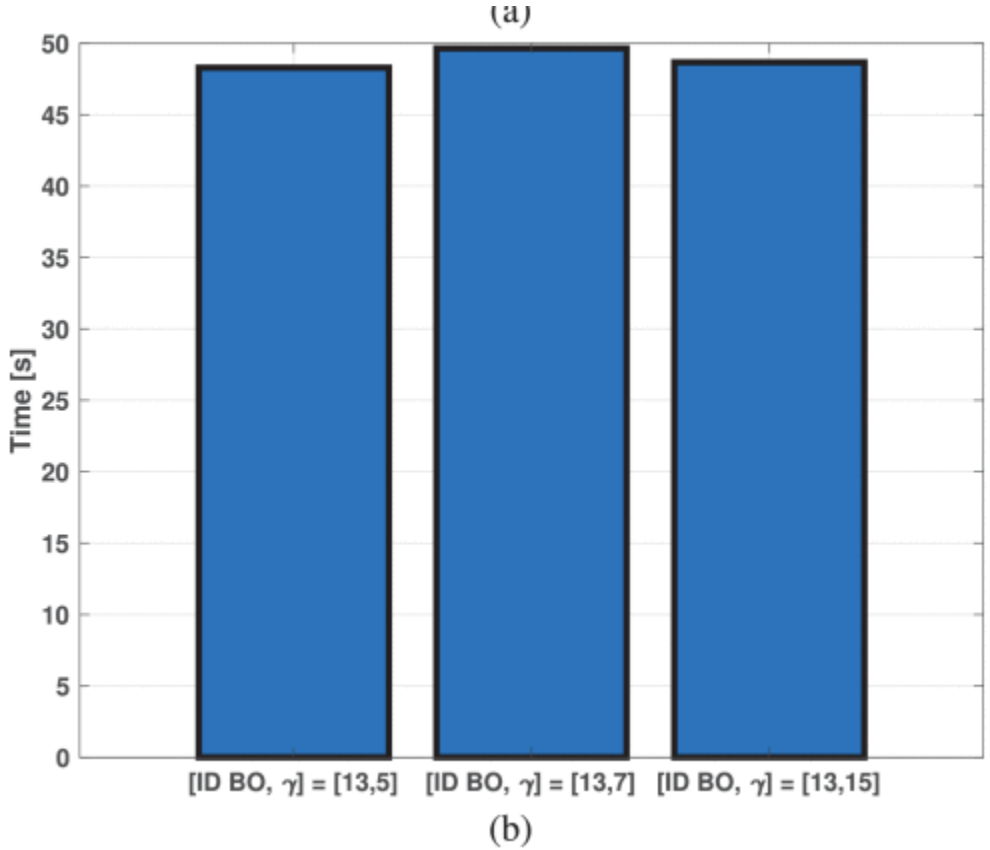

Image | Comment

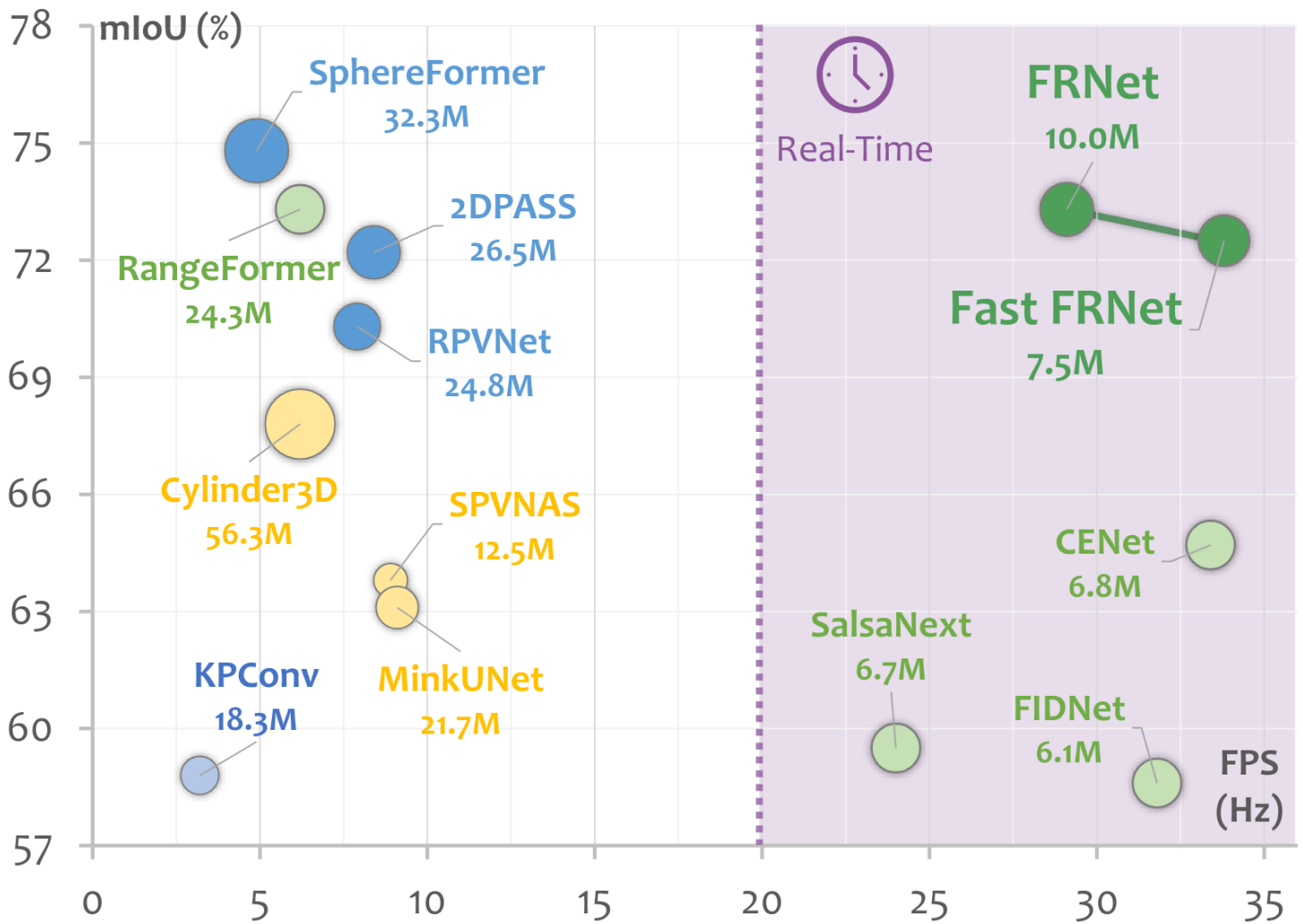

Image	Comment

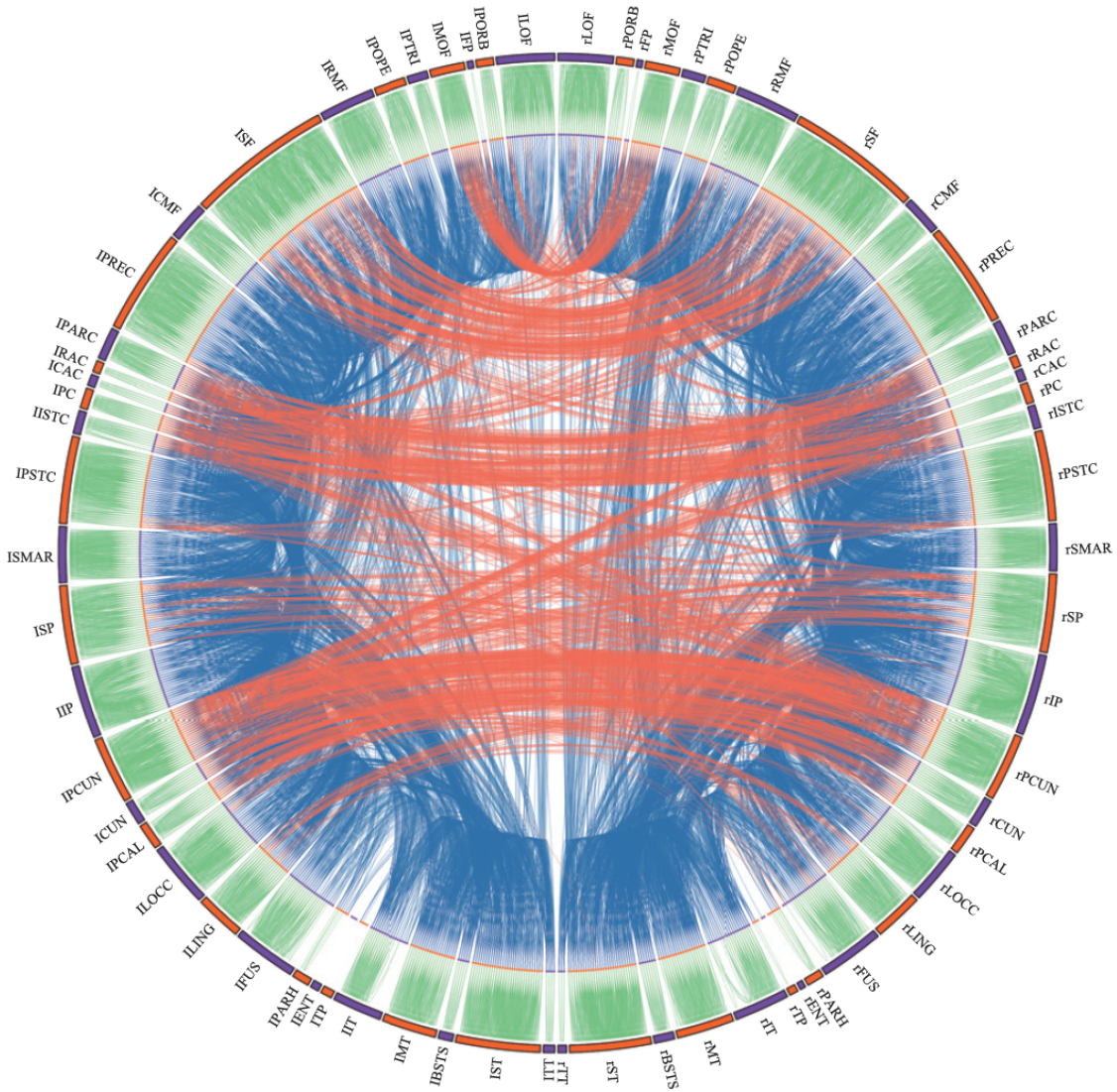
lLOF
rLOF
rPORB
rFP
rMOF
rPTRI
rPOPE
rRMF
rSF
rCMF
rPREC
rPARC
rRAC
rCAC
rPC
rISTC
rPSTC
rSMAR
rSP
rIP
rPCUN
rCUN
rPCAL
rLOCC
rLING
rFUS
rPARH
rENT
rTP
rIT
rMT
rBSTS
rST
lST
lLT
rLT
lBSTS
lMT
lIT
lTP
lENT
lPARH
lFUS
lLING
lLOCC
lPCAL
lCUN
lPCUN
lIP
lSP
lSMAR
lPSTC
lISTC
lPC
lCAC
lRAC
lPARC
lPREC
lCMF
lSF
lRMF
lPOPE
lPTRI
lMOF
lFP
lPORB

Image | Comment

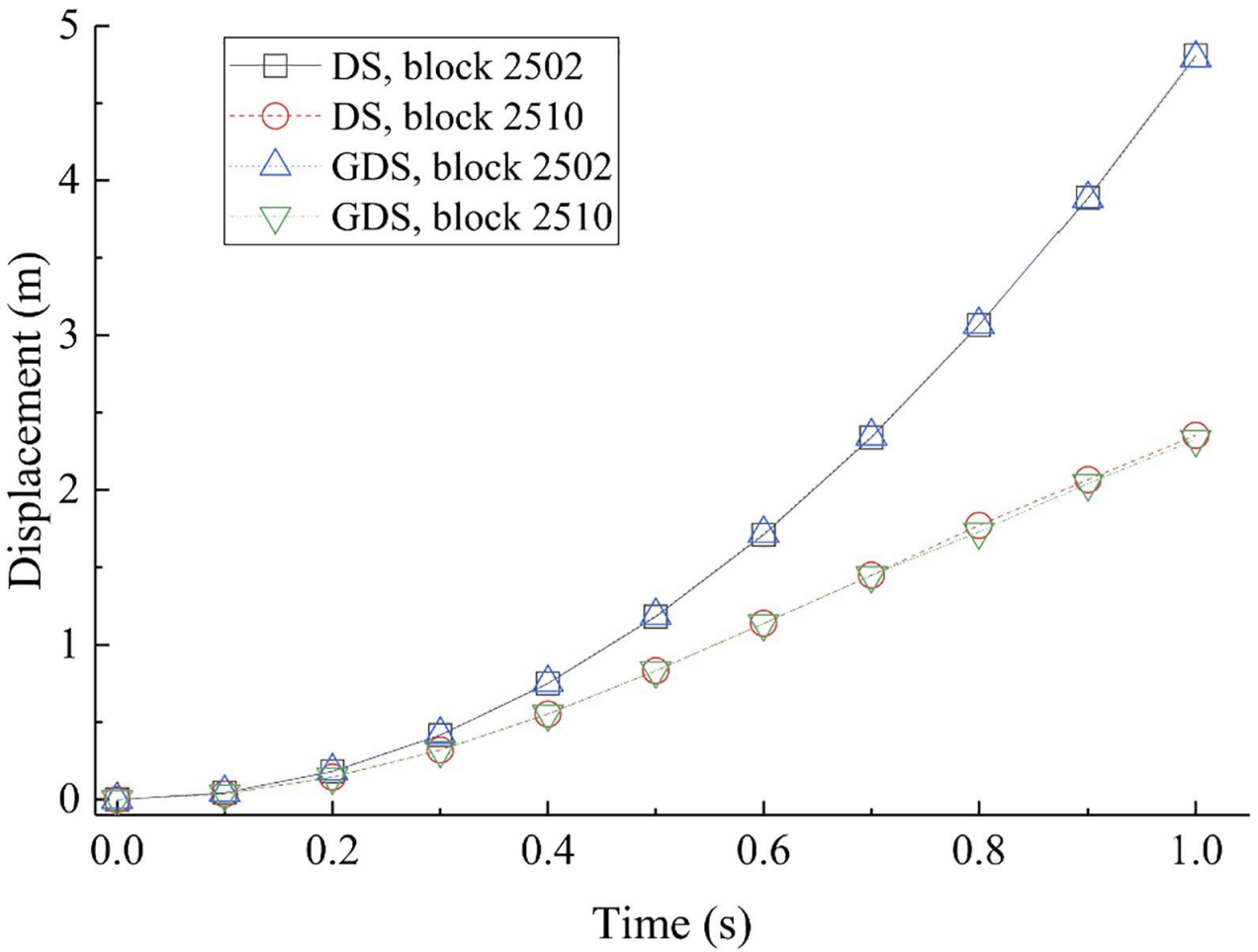

Image | Comment

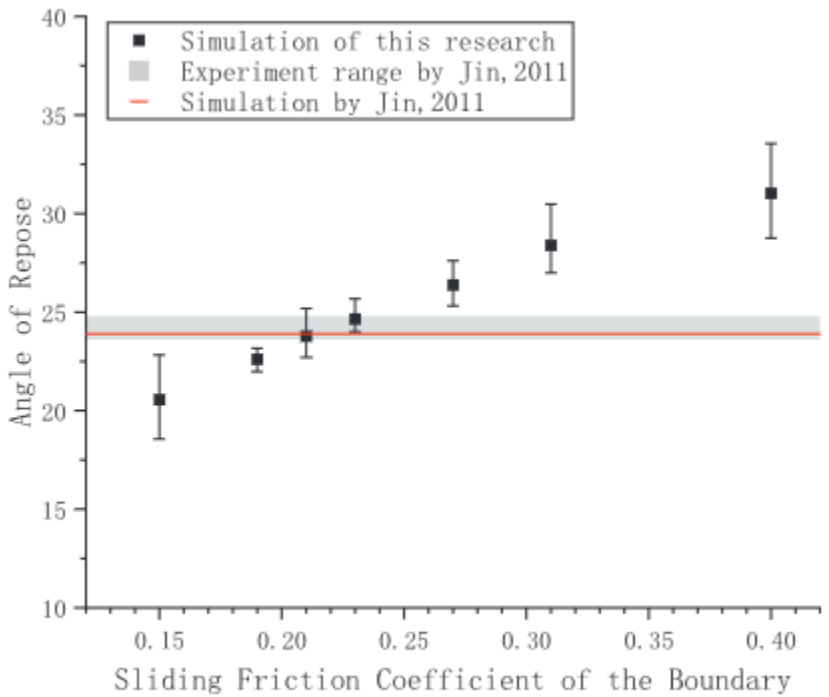

Fig. 11. The angle of repose varies with the boundary sliding friction coefficient and is compared with the experimental result.

Image	Comment

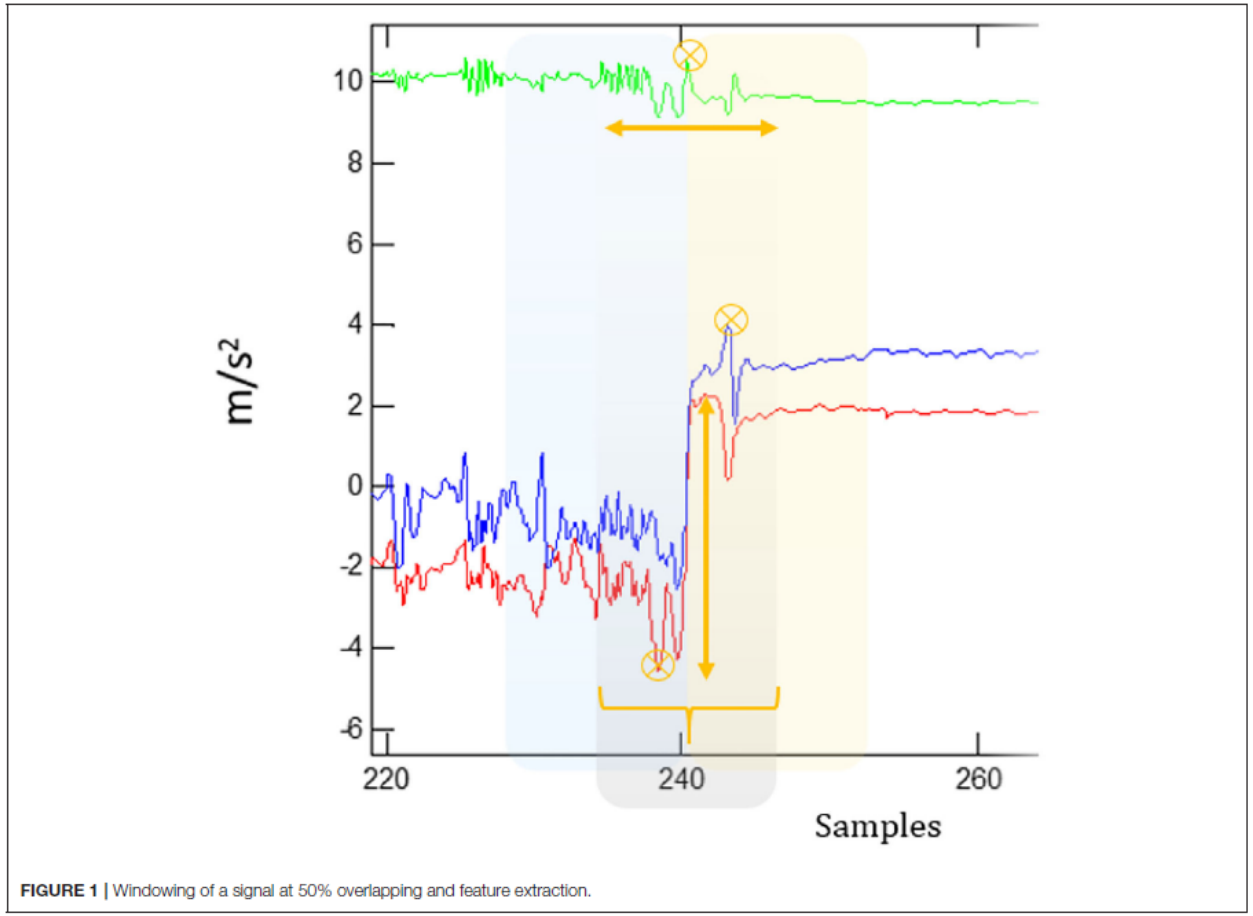

FIGURE 1 | Windowing of a signal at 50% overlapping and feature extraction.